Geoarchaeology

WILEY

Geoarchaeology An International Journal

RESEARCH ARTICLE OPEN ACCESS

The Neolithic Site of Piano dei Cardoni in the Island of Ustica (Italy): Minero-Petrographic and Chemical Characterization of the Ceramic Finds and Clayey Raw Materials

G. Montana[1] | C. Speciale[2,3] | G. Battaglia[4] | L. Randazzo[1,5] | G. Carnevale[5] | M. V. Antonopoulou[6] | A. Magrì[7]

[1]Department of Earth and Marine Sciences (DiSTeM) - University of Palermo, Palermo, Italy | [2]Department of Biological, Chemical and Pharmaceutical Sciences and Technologies (STeBiCeF), University of Palermo, Palermo, Italy | [3]IPHES-CERCA, Catalan Institute of Human Paleoecology and Social Evolution, Tarragona, Spain | [4]Soprintendenza dei Beni Culturali e Ambientali, Palermo, Italy | [5]Istituto Nazionale di Geofisica e Vulcanologia (INGV) – Sez, Palermo, Italy | [6]Department of Geology - University of Patras (Greece), Patras, Greece | [7]Department of Classics and Archaeology, Faculty of Arts - University of Malta, Msida, Malta

Correspondence: C. Speciale (claudia.speciale@unipa.it)

Received: 11 November 2024 | **Revised:** 5 February 2026 | **Accepted:** 21 February 2026

Scientific Editor: Kevin Walsh and Helen Mackay

Funding: European Union's Horizon 2020 research and innovation program MSCA-COFUND R2STAIR, Grant/Award Number: 101034349; Spanish Ministry of Science, Grant/Award Number: CEX2019-000945-M

Keywords: 5th millennium BCE | archaeometry | Island of ustica | neolithic | pottery technology | Sicily

ABSTRACT

This paper presents the results of minero-petrographic and chemical analyses of pottery and potential local raw materials from Ustica, a small volcanic island off the coast of Palermo (Sicily), inhabited during the Middle Neolithic. Typologically, the pottery shows cultural connections to the *Bicromica* and *Serra d'Alto* traditions, linking Ustica to Sicily and Southern Italy, as well as to the Late Neolithic *Diana* pottery from the Aeolian Archipelago. The archaeometric study aims to determine whether the island's inhabitants during the 5th millennium BCE engaged in the exchange of ceramics in addition to obsidian and chert. This research investigates raw material sources, technological knowledge, and pottery-making traditions on the island by analyzing the compositional, textural, and structural characteristics of the ceramic assemblage. The experimental results indicate the use of local raw materials from areas near the archaeological site and provide insights into firing techniques, helping to establish the petrographic and chemical profiles of the ceramics. These findings contribute to a broader understanding of Neolithic pottery production in the central Mediterranean.

1 | Introduction

Ustica is a small volcanic island of approximately 9 km^2, off the northwestern coast of Sicily, near Palermo. Human occupation of the island dates back to the late 6th to early 5th millennium BCE, when human communities—likely originating from the Palermo area or the Aeolian Islands—chose to settle there, probably to exploit and facilitate the transport of obsidian from Lipari (Aeolian Islands) to western Sicily (Speciale, Freund et al. 2021; Speciale, Montana et al. 2021).

Mobility and resource use on islands are recurring themes in archaeological research focused on insular environments. Building on the foundational principles of island biogeography—where ecological dynamics are largely governed by island size and distance from the mainland (MacArthur and Wilson 2016)—archaeologists have adapted several of these models to human behavior (DiNapoli and Leppard 2018). Islands are inherently subject to fluctuating patterns of occupation and abandonment, particularly when they are small and remote (Dawson 2016). Maritime navigation and technological knowledge of seafaring are therefore crucial for understanding early human occupations and the diverse forms that they may take, ranging from sporadic, one-off landings and occasional visits, to permanent and organized settlement and exploitation of the island's resources. Nonetheless, specific geographic features or the presence of unique resources—especially during prehistory—can render certain islands more attractive than others, even when they are very remote or resource-scarce, such as in the case of limited freshwater availability.

The Middle Neolithic settlement of Ustica—a small and seasonally isolated landmass—was likely inhabited year-round. Several lines of archaeological evidence support this hypothesis: (1) the presence of agricultural tools made from local volcanic rock, along with archaeobotanical remains (Speciale, et al. 2023); (2) a rich and diverse zooarchaeological assemblage, including domestic and wild terrestrial, marine, and aerial fauna (Prillo et al. 2021); and (3) the $^{87}Sr/^{86}Sr$ isotope values from human bones, pigs, and ovicaprines, which closely align with local water—collected from the seasonal ponds and inside a cave—and soil baselines (Speciale et al. in press). Cultural comparisons further situate the Piano dei Cardoni site within a broader context, revealing links to Southern Italy in both burial architecture and ceramic decoration styles (Magrì et al. 2023). Additionally, the widespread presence of Lipari obsidian and chert tools—whose origins remain uncertain but are definitively nonlocal—places Ustica within a broader network of raw material procurement and/or exchange spanning at least the southern Tyrrhenian region (Speciale, Montana, et al. 2021).

Although limited by a fragmentary context and a low percentage of reconstructable vessel shapes, the ceramic assemblage from Piano dei Cardoni comprises four main classes, distinguished by macroscopic technological features and surface treatments (Magrì et al. 2023): (1) coarse wares with smoothed surfaces; (2) dark burnished ceramics, occasionally decorated with incised or excised motifs; (3) red burnished pottery; and (4) red-painted ceramics on reserved or white backgrounds (red-on-white). The vessels are hand-modeled and have simple forms, including medium and small jars, large deep bowls, shallow small bowls, and miniature vessels. The provenance of the ceramics from Piano dei Cardoni remains an open question. From a cultural perspective, the assemblage includes elements of the Late Neolithic *Diana* pottery group, notably red or coral burnished wares with characteristic spool-shaped handles—types widely attested in the Aeolian Archipelago (Martinelli 2020). The significant presence of red-on-white painted ceramics, associated with the broader *Bicromica* and *Serra d'Alto* traditions, links Ustica not only to the Aeolian Archipelago and Sicily but also to Southern Italy. Therefore, the characterization of ceramic provenance is of critical importance in this context. Archaeometric analyses of these ceramics can clarify whether Ustica's early settlers—likely the first permanent inhabitants of the island between the late 6th and mid-5th millennium BCE—were trading materials other than obsidian and chert.

Given the extensive networks characterizing northwestern Sicily during the Middle and Late Neolithic, and the likelihood of temporary mobility among Ustica's inhabitants, imported pottery could theoretically have originated not only from the Aeolian Islands but also from the Palermo coast or even farther east.

Another key question concerns the technological capabilities of the community, in the case of local production. On a small and seasonally isolated island like Ustica, resource exploitation and management would have been crucial for the survival of local communities. Did the inhabitants know where to find suitable clay deposits? Did the island's volcanic soils require specific preprocessing before shaping vessels? Were distinct (and locally available) raw materials intentionally selected for the different ceramic classes?

Answering these questions can help evaluate whether the island's Neolithic occupation was marked by stability or mobility, and whether the community was self-sufficient or dependent on external resources.

Furthermore, such insights can shed light on the community's knowledge of local geology and the potential development of a ceramic production tradition. This includes the *chaîne opératoire* of pottery-making, and whether it implies the presence of highly skilled artisans—capable, for instance, of controlling firing temperatures and kiln structures.

Unfortunately, microscopic fabric analyses of Neolithic ceramics are still relatively rare in Sicily and the surrounding islands (Levi and Muntoni 2014), especially when compared to other regions such as Apulia (Muntoni and Laviano 2008; Laviano and Muntoni 2011). Notable exceptions include Mannoni's early work on Neolithic pottery fabrics from Lipari (1980), the recent study by (Levi et al. 2020) and the one on the pigments from Neolithic sites in the Aeolian islands (Armetta et al. 2023).

In recent decades, archaeometric methods and techniques applied to the study of ceramic fabrics have significantly progressed, allowing for a more precise understanding of materiality, technological and cultural traditions, and the processes of learning and transmission (Albero Santacreu 2014; Roux 2019; Amicone et al. 2019; Giligny et al. 2021).

At the current stage of research, Neolithic painted pottery is widely recognized as a notable example of highly specialized ceramic production. This technological sophistication is evident in the deliberate selection and meticulous control of raw materials, as well as in the use of advanced firing techniques. The systematic application of specific pigment types across various Mediterranean cultural areas further highlights the technological proficiency of Neolithic potters, reflecting the rise of skilled craftsmanship within increasingly structured societies (Angeli et al. 2018; Laviano and Muntoni 2009; Capel et al. 2006).

In this context, the case of Ustica may serve as a significant point of reference for understanding ceramic production and technology in the Central Mediterranean during the Middle to Late Neolithic. To address the questions previously posed, potential ceramic raw materials were sampled from residual soils at the Piano dei Cardoni site and other locations across the island. These materials were then analyzed using a comprehensive multi-instrumental approach from both mineralogical–petrographic and chemical perspectives, including post-firing characterization, following experimental firings at 700°C in an oxidizing atmosphere.

The choice of the firing temperature was informed by previous research on ceramic materials from the same site (Speciale, Montana, et al. 2021). The fired test samples were subsequently compared with the different ceramic typologies identified at Piano dei Cardoni. This comparison aimed to provide insights into the production processes and technological practices, and to further refine the petrographic and chemical markers of local Neolithic pottery.

2 | Archaeological Background and Ceramic Materials

The site of Piano dei Cardoni is located on the southern coast of Ustica and represents the earliest known permanent human occupation of the island (Speciale, Freund, et al. 2021; Speciale, Montana, et al. 2021). Survey activities conducted in 2017 and 2018 identified a settlement area of approximately 2 ha, which was partially investigated during excavation campaigns between 2018 and 2020 through three test trenches (Trench 1, 2, and 3) (Speciale et al. 2019; Speciale et al. 2022; Speciale et al. 2023). Piano dei Cardoni comprises a large burial complex with evidence of multiple phases of use.

The primary archaeological feature uncovered in Trench 2 is a megalithic hypogean funerary structure consisting of an oval pit (approximately 2 × 1 m), excavated into the clay substrate and lined with nine vertically placed volcanic slabs, each about 80 cm high (Figure 1B). The burial chamber, originally accessible through a lateral opening, was later sealed from above with a massive slab weighing several tons. Secondary bone deposits were found within the burial chamber, above the cover slab, and in its immediate surroundings, indicating the structure's prolonged use over several centuries. These secondary deposits, referred to as "bone clusters," were sometimes placed within small depressions; in other cases, they appear to have resulted from unintentional or scattered deposition within confined areas.

Eight AMS radiocarbon dates, obtained from selected faunal and human bones recovered during the 2019–2020 excavation campaigns, correspond to four stratigraphically defined phases. These results confirm the chronology previously inferred from ceramic assemblages, dating to the mid-5th millennium BCE (Speciale et al. 2024).

The ceramic assemblage analyzed in this study derives primarily from Trench 2 (18 samples), specifically from the layers within the burial chamber and its surrounding area, where ceramics were found in association with external bone clusters.

An additional set of ceramic samples (10) comes from Trench 3, where occupation layers potentially related to the use of the funerary structure were identified during the 2020 excavation campaign (Table S1A,B).

As previously noted, the pottery assemblage from Piano dei Cardoni comprises a limited range of vessel forms, all in a fragmentary state of preservation. Functionally, the majority of the vessels are tableware used for food consumption—mainly shallow and deep bowls of medium to small size. Storage vessels (jars and small jars) are also present, albeit in smaller quantities. Coarse wares are scarce, and cooking vessels are nearly absent, consistent with the funerary and ritual nature of the context. From a chronocultural perspective, the pottery from Piano dei Cardoni spans from the Middle to the Late Neolithic. It includes parallels with several well-known Sicilian ceramic traditions: Kronio wares (characterized by incised or excised decoration), Diana wares (red and brown burnished surfaces), and the bichrome-painted ceramics (red-on-whitish slip, bicromica), the latter representing a significant component of the site's assemblage (Figure 2). A schematic summary of the analyzed samples, categorized by vessel morphology (open vs. closed forms) and surface treatment, is presented in Table 1.

Among the closed forms (Table 1), two main types can be distinguished: vessels with light red to bright coral surfaces, ranging from smoothed to highly polished (i.e., red-lustrous wares), and vessels with darker reddish-brown to brown surfaces, typically smoothed or poorly burnished. Within the open forms (Table 1), which consist almost entirely of bowls varying in size and depth, examples include red or reddish vessels that are consistently polished, as well as bowls with a white slip decorated with red painted motifs. A key research question regarding the red polished vessels is whether the lustrous finish was achieved by manual burnishing (e.g., with a stick or similar tool) or through the application of a thin, glossy clay-based slip (Figure 2). In some cases, even among vessels with opaque red, dark reddish, or brown surfaces, macroscopic observation of smoothed areas reveals traces of former polishing, likely no longer preserved due to post-depositional processes.

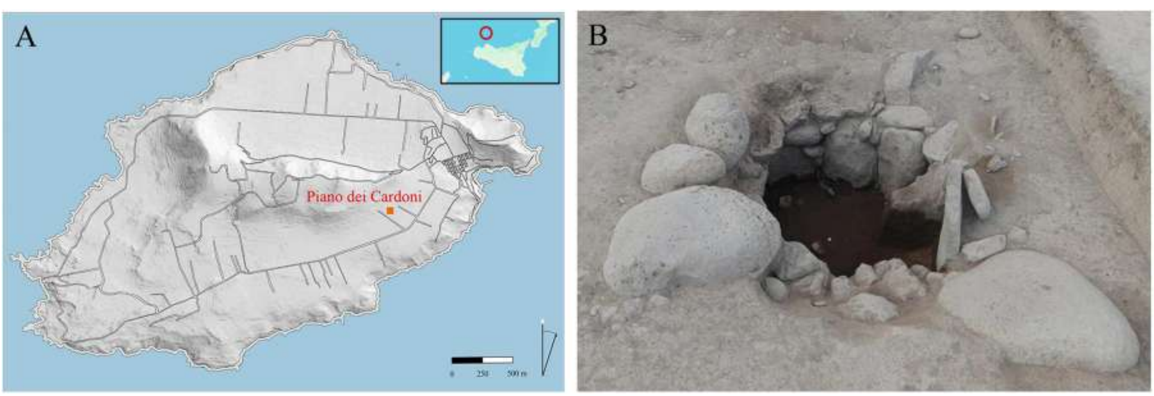

FIGURE 1 | (A) The Island of Ustica and the site of Piano dei Cardoni on the southern coast. (B) The semi-hypogeic structure of the Neolithic tomb.

FIGURE 2 | Piano dei Cardoni, Ustica. Selection of ceramic samples examined in this paper: (1) UCRD_9, Jar with a Diana handle. (2) UCRD_24, Jar with a Diana handle. (3) UCRD_26, Small jar with a Diana handle. (4) UCRD_30, Jar. (5) UCRD_23, Jar. (6) UCRD_10, Large deep bowl. (7) UCRD_22, Painted deep bowl. (8) UCRD_21, Painted bowl. (9) UCRD_25, Diana bowl. (10) UCRD_17, Painted bowl. (11) UCRD_16, Painted bowl. (12) UCRD_12, Diana shallow bowl. (13) UCRD_18, Painted bowl. (14) UCRD_28, Painted bowl (the sherds with micrite lumps are marked with red circles; scale 1:6) (drawings: A. Magrì).

3 | Geological Sketch and Clayey Raw Materials' Sampling

Ustica is a volcanic island located in the southern Tyrrhenian Sea, formed through multiple eruptive episodes that occurred between the early and late Pleistocene. The island is predominantly composed of volcanic rocks, with only minor sedimentary deposits resulting from more recent marine terrace formations (Figure 3A).

Volcanic rocks display a Na-alkaline affinity and range in composition from alkali basalts to alkali trachytes. They are mainly classified as basalts (including hawaiites and mugearites) and trachytes, produced by both subaqueous and subaerial eruptions, in either effusive or explosive regimes. The sedimentary deposits, which formed during the middle to upper Pleistocene glacio-eustatic sea-level high-stands, are distributed along the island's coastline. These deposits include fossiliferous conglomerates, breccias, variably cemented sands, and organogenic and concretional calcareous layers. Additionally, reworked volcanogenic materials and paleosols frequently cover erosional surfaces across the island (de Vita 1993; de Vita and Foresta Martin 2017; de Vita et al. 1998; Bonomo and Ricci 2010).

The study area is located in the eastern part of Ustica, at Piano dei Cardoni, a flat landform representing an erosional surface associated with a transgressive–regressive cycle of Crotonian age, developed over older submarine and subaerial lava flows (Martin and Furlani 2021; Speciale, Montana, et al. 2021). The Piano dei Cardoni lowland extends an ENE-WSW–trending strip of land, roughly parallel to the island's central ridge, at elevations ranging from 80 to 120 m a.s.l., with an average slope of approximately 5%. The terrace gently dips eastward, a consequence of quaternary tectonic displacement (de Vita et al. 1995; 1998).

Regarding sampling, eight Holocene clayey soil samples were collected from different locations across Ustica, but only four were finally considered suitable for the analyses.

TABLE 1 | Piano dei Cardoni. Distribution of the samples related to closed and open shapes.

Jars				**Small Jar**
				
UCRD_7 Tr. 3, SU 1037, sq. C Wall fragment with a Diana-type handle. Smoothed surfaces.	**UCRD_6** Tr. 3, SU 1037, sq. C Rim fragment. Red burnished surf.	**UCRD_30** Tr. 2, SU 9, sq. L Rim Fragment. Smoothed surfaces.	**UCRD_4** Tr. 3, SU 1041, sq. A Rim fragment. Smoothed surfaces.	**UCRD_26** Tr. 2, Profile clean., sq. H Rim fragment with a Diana-type handle. Slightly burnished surf.
UCRD_9 Tr. 3, SU 1027, sq. A-B Wall fragment with a Diana-type handle. Smoothed surfaces.	**UCRD_24** Tr. 2, SU 47, sq. DD Rim fragment with a Diana-type handle. Burnished surfaces?		**UCRD_23** Tr. 2, SU 51, sq. I Rim fragment. Smoothed surfaces.	
UCRD_14 Tr. 2, SU 38, sq. L Wall fragment. Smoothed surfaces.				
Large Bowls	***Bowls***		***Painted Bowls***	
				
UCRD_10 Tr. 2, SU 48, sq. CC Rim fragment. Burnished surfaces.	**UCRD_25** Tr. 2, SU 28, sq. I Rim fragment. Red burnished surf.	**UCRD_12** Tr. 2, SU 47, sq. CC Wall fragment. Red burnished surf.	**UCRD_5** Tr. 3, SU 1037, sq. C Rim fragment. Red-on-light painted.	**UCRD_1** Tr. 3, SU 1030, sq. B Base fragment. Red-on-light painted.
			UCRD_11 Tr. 2, SU 29, sq. CC Wall fragment. Red-on-light painted.	**UCRD_2** Tr. 3, SU 1037, sq. B Rim fragment. Red-on-light painted.
			UCRD_13 Tr. 2, SU 51, sq. I Wall fragment. Red-on-light painted.	**UCRD_3** Tr. 3, SU 1037, sq. C Rim fragment. Red-on-light painted.
			UCRD_15 Tr. 2, SU 38, sq. L Wall fragment. Red-on-light painted.	**UCRD_8** Tr. 3, SU 1037, sq. C Wall fragment. Red-on-light painted.
			UCRD_22 Tr. 2, SU 46, sq. I Wall fragment. Red-on-light painted.	**UCRD_16** Tr. 2, SU 38, sq./ Rim fragment. Red-on-light painted.
			UCRD_27 Tr. 2, SU 25, sq. DD Base fragment. Red-on-light painted.	**UCRD_17** Tr. 2, SU 29, sq. CC Rim fragment. Red-on-light painted.
			UCRD_28 Tr. 2, SU 47II, sq. CC Red-on-light painted.	**UCRD_18** Tr. 2, SU 48, sq. CC Rim Fragment.
				UCRD_21 Tr. 3, SU 1027, sq. A-B Wall Fragment.
				UCRD_29 Tr. 2, SU 47II, sq. CC Wall Fragment.

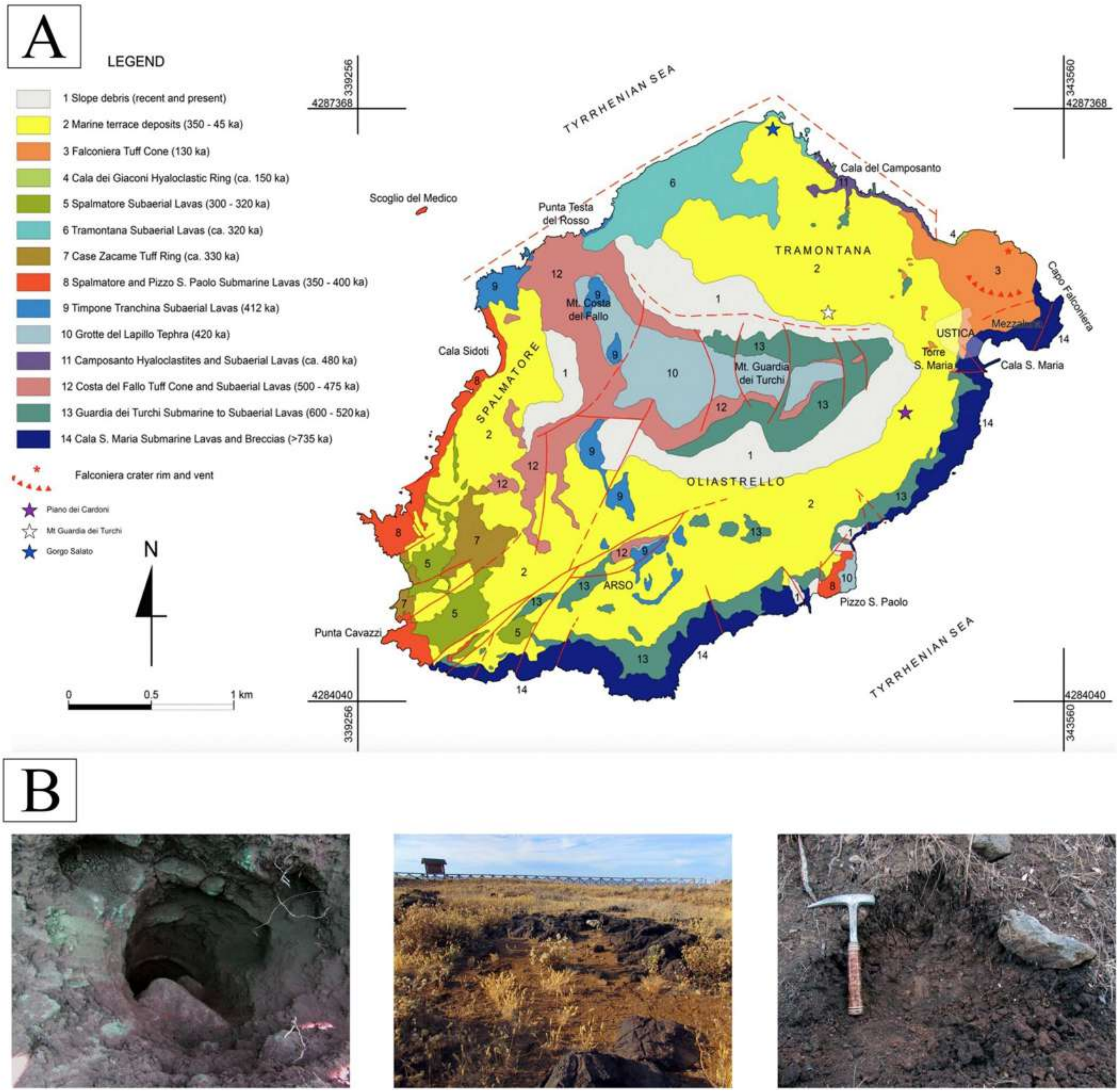

FIGURE 3 | (A) Geological map of Ustica modified after de Vita and Foresta Martin (2017). (B) Sampling point of clayey raw materials, from left to right, respectively, Piano dei Cardoni, Gorgo Salato, and Monte Guardia dei Turchi.

These sandy–clayey sediments originate from the weathering of volcanic materials (lava flows and pyroclastic deposits) as well as the previously cited Upper Pleistocene terraced sedimentary deposits. Two of these samples originate from the Piano dei Cardoni area (UST_4 and UST_XYZ).

Sample UST_4, pale gray in color, was taken directly from the current soil surface, after carefully removing the most recent layers. In contract, sample UST_XYZ, yellowish-brown in color, was collected at a depth of 1.5 from an archaeological excavation, representing Neolithic paleosol. Sample UST_5, dark brown in color, was collected from the Gorgo Salato area, whereas sample UST_7, reddish brown, was collected from the Northern part of the island (Sentiero Tramontana along Monte Guardia dei Turchi) (Figure 3B).

4 | Analytical Procedure and Methods

Analytical techniques were used not only to characterize the composition of the clayey materials and prehistoric ceramics but also to define key technical features related to the production process. For example, grain size distribution and the volumetric abundance of sand-sized aplastic inclusions can significantly influence the plasticity and overall workability of the clay raw materials selected for ceramic production. These features also help predict the performance of the finished ceramic objects in relation to their intended use. Consequently, the analytical results enable verification of the provenance (local vs. imported) of the new ceramic samples collected at Piano dei Cardoni and allow assessment of the criteria used for raw material selection on the island during the Neolithic period. Interpretation of compositional, textural, and structural data, obtained through multi-instrumental analysis of local clayey raw materials (after experimental firing) alongside archaeological ceramic samples, provides a preliminary evaluation of the technological level achieved at the site.

The raw clayey samples were first air-dried at room temperature for 1–2 weeks, and then gently disaggregated using a porcelain mortar and wooden pestle to avoid fracturing larger aplastic granules. After careful quartering, representative amounts were subjected to grain size analysis. Samples were separated into a coarse fraction (particles between 2 and 0.06 mm) and a fine fraction (particles < 0.06 mm) using a settling cylinder following Stoke's Law. The fine fraction was further divided into silt (0.06–0.002 mm) and clay (< 0.002 mm) by centrifugation at 2000 and 4000 rpm, respectively. These fractions were dried in a ventilated oven at 60°C for 48 h, equilibrated at room temperature over silica gel, and weighed on an analytical balance. Suspensions of clay particles in distilled water were preserved for potential future use in X-ray powder diffraction (XRPD) analyses of clay phyllosilicates.

For experimental firing, 50 g of air-dried clay was homogenized and mixed with water to reach optimal plasticity. Small briquettes (two per sample, measuring 40 × 15 × 15 mm) were shaped using wooden molds, dried in a ventilated oven at 60°C, and fired in a muffle furnace at 700°C at a heating rate of 200°C/h and a soaking time of 1 h under an oxidizing atmosphere. After cooling, fired briquettes were embedded in epoxy resin, thin-sectioned, and examined under a polarizing microscope for comparison with archaeological ceramics (Montana 2020).

Mineralogical and petrographic observations of archaeological ceramics were performed on standard thin sections using a Leica DM LSP polarizing microscope equipped with a digital camera (Leica DC 200). The relative abundance of non-plastic inclusions (expressed as area %) was estimated using established comparative tables (Matthew 1991). Experimental briquettes were examined using the same methods.

XRPD analyses were carried out on both fired experimental briquettes and archaeological ceramic samples using a PANalytical X'PERT PRO diffractometer with a Cu anode, a graphite monochromator, operating at 40 kV and 30 mA. Scans were recorded over a 2θ range of 5°–60° at a rate of 2°/min with a 2-s time constant. Mineralogical phase identification was performed with PANalytical X'Pert software by matching diffraction patterns to the 2005 PDF2 reference database.

Bulk chemical compositions of selected ceramics (13 of 28 samples) and clayey samples (4) were analyzed at Activation Laboratories Ltd. (Ontario, Canada) using fusion inductively coupled plasma optical emission spectrometry (ICP-OES) and inductively coupled plasma mass spectrometry (ICP-MS) (Thermo Jarrell-Ash ENVIRO II ICP and Varian Vista 735 ICP). Details on analytical protocols and sensitivity for the 55 chemical determined elements are provided in Montana et al. (2022).

Scanning electron microscopy coupled with energy-dispersive spectroscopy (SEM-EDS) was conducted on fresh fractured surfaces of both unfired and fired clay materials to observe structural transformations after firing. The same technique was applied to ceramic artifacts to assess sintering degree and textural/compositional features. Spot chemical analyses of aplastic inclusions were also performed. SEM-EDS were conducted at the Advanced Technologies Network Center (ATeN), University of Palermo, using a Phenom Pro Desktop SEM (CeB_6 detector, resolution < 5 nm) equipped with an EDS spectrometer for microchemical characterization.

5 | Results

5.1 | Clayey Raw Materials

5.1.1 | Grain Size Analysis

The results of the granulometric analysis are reported in Figure 4, in which the relative proportions of sand (> 62.5 μm), silt (4–62.5 μm), and clay (< 4 μm) of the collected clayey materials are shown. The proportion of the sand fraction is widely distributed over a range of 1% (very few) to 17% (sporadic). The silt fraction shows a relatively smaller variation and it is distributed between 41% and 48%, whereas the clay fraction fluctuates between 40% and 51%. According to Shepard's classification scheme (Shepard 1954), all the samples can be classified as silty clays with common to sporadic and rare sand-sized aplastic inclusions (Figure 4).

5.1.2 | XRPD Analysis

The evaluation of the X-ray patterns led to division of the clayey soil samples collected in Ustica (i.e., potential ceramic raw materials) into two "classes," according to the semi-quantitative determination of the crystalline phases on the powdered *tout venant*. Half of the analyzed samples (UST_5 and UST_7) were characterized by the absence of calcite both before and after firing tests. This result can be relatively expected, considering that these are colluvial deposits formed on geologically recent aerial volcanic products. On the contrary, samples UST_4 and UST_XYZ showed the presence of minor to relevant quantities of calcite. This result is theoretically rather surprising, given that the presence of calcite, at least in marine clays, is largely correlated with the abundance of planktonic and benthic calcareous-shelled foraminifers, which are totally absent in Ustica's volcanic deposits, as well as in their derived aerial weathering products.

Particularly, using X-ray diffraction, the mineralogical composition of the samples UST_5 and UST_7 was, in decreasing order of abundance, as follows: quartz, plagioclase, K-feldspar, illite, clinopyroxene, and hematite (Table 2). Quartz seems to be the most abundant mineral in these samples (stronger diffraction effects) as well as the plagioclase. Alkaline feldspar and illite are common to sporadic regarding the intensity of their diagnostic reflections. Clinopyroxene was detected only as sporadic to rare (Figure 5). Some indicative d-spacings of the main reflections for the quartz found in the samples are 3.34, 4.26, 2.46, and 2.28 Å. Plagioclase and K-feldspar are recognized at 3.19, 4.03, 3.68, and 3.22 Å, and 4.22, 3.31, and 3.24 Å, respectively. The characteristic *d* spacings for illite are 10, 4.97, 4.47, and 3.72 Å, whereas for hematite, the characteristic

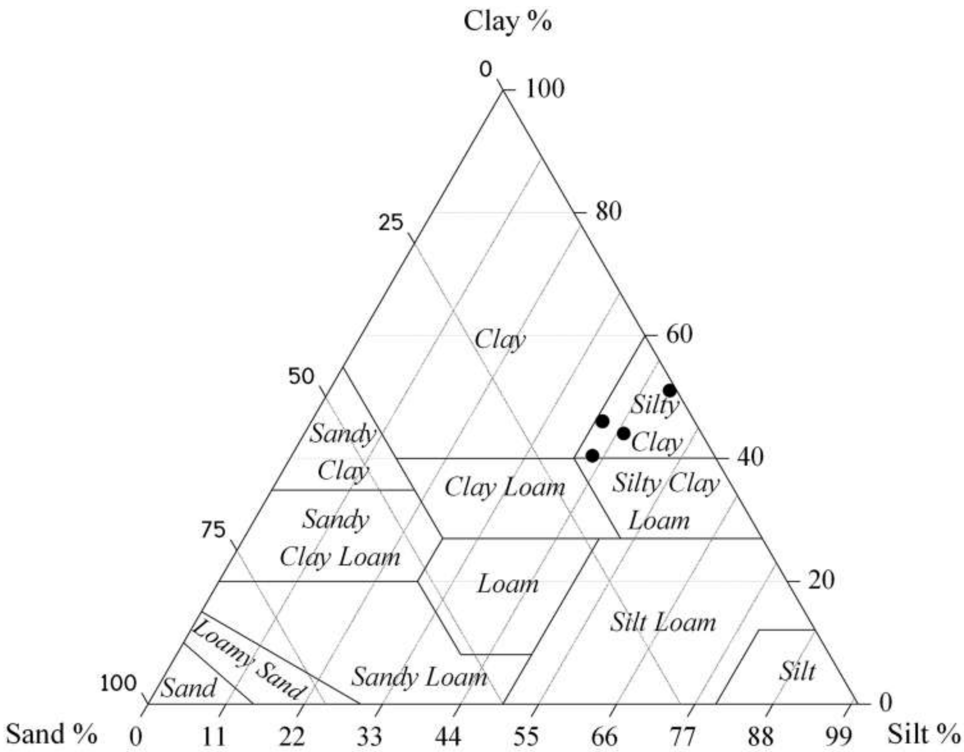

Sample code	Sand (%)	Silt(%)	Clay(%)
UST_4	17	41	42
UST_XYZ	11	44	45
UST_5	1	48	51
UST_7	13	41	46

FIGURE 4 | Classification of the clayey samples according to their grain size distribution and their projection on the Shepard diagram (Shepard 1954).

TABLE 2 | Results of XRPD analysis.

	Sample code	T (°C)	Qz	Pl	Afs	Ill + I/S	Cpx	Cc	Hm
Without PML	UST_5	Air-dried leather-hard brick	+++	++	+	++	tr	—	tr
		Brick-fired at 700°C	+++	++	+	++	tr	—	+
	UST_7	Air-dried leather-hard brick	++	+++	+	++	+/tr	—	tr
		Brick-fired at 700°C	++	+++	+	++	+/tr	—	+
With PML	UST_4	Leather-hard brick	+++	+++	+	++	tr	+/tr	—
		Brick-fired at 700°C	+++	+++	+	++	tr	tr	tr
	UST_XYZ	Leather-hard brick	+++	++	+	++	+/tr	++	—
		Brick-fired at 700°C	+++	++	+	++	+/tr	++/+	tr

Note: Qualifiers legend: +++, abundant; ++, common; +, sporadic; tr, traces; —, not detected. Abbreviations: Afs, alkaline feldspar; Cc, calcite; Cpx, clinopyroxene; Hm, hematite.Ill + I/S, illite and mixed layer Illite/smectite; Pl, plagioclase; PML, pedogenic micrite lumps; Qz, quartz.

d spacing is 2.69 Å. Only sample UST_7 shows the presence of mixed layers I/S (Table 3).

The mineralogical composition of samples UST_4 and UST_XYZ is overall very similar to the previous ones. It differs merely in the presence and relative abundance of calcite (Figure 5A,G), with the d-spacings of the main reflections at 3.04, 3.86, 2.49, 2.28, and 2.10 Å.

After firing the clayey raw materials at 700°C, the mineralogical modifications are not significant. Particularly, the plagioclase is more frequent than that in the unfired samples and hematite's strongest peak is now evident (Figure 5B). Calcite persists up to 700°C (even if showing a lower reflection intensity) and identifying peaks of Illite are still present at the same temperature (Figure 5H).

5.1.3 | *Thin-Section Microscopy and Chemical Analysis of Firing Tests*

At first glance, all samples show clear similarities in both textural and compositional characteristics. Regarding texture, they show a heterogeneous distribution and systematic sorting of

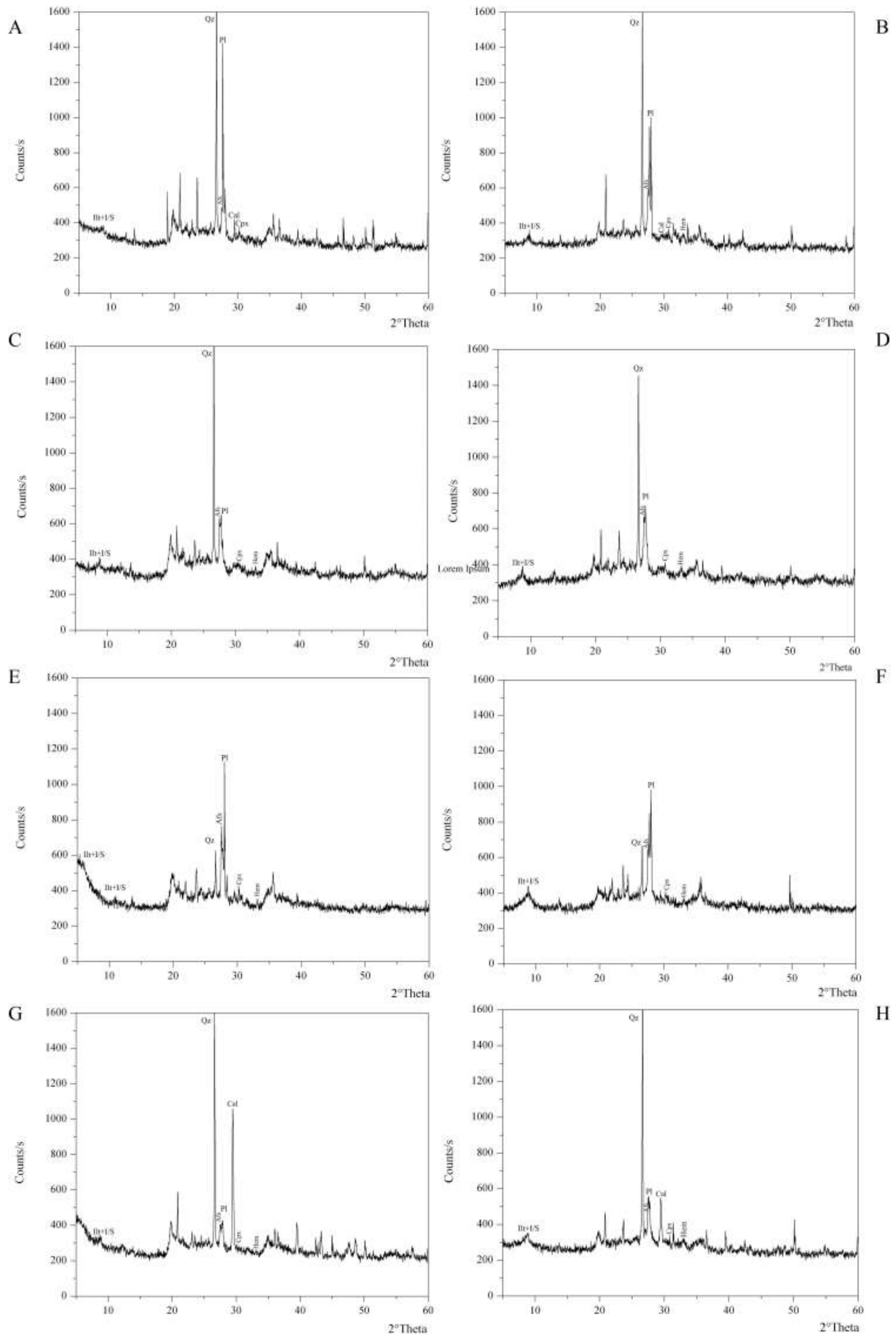

FIGURE 5 | X-ray diffractograms and evaluation of the unfired and fired material at 700°C: (A, B) UST_4 and UST_4 _700; (C, D) UST_5 and UST_5 _700; (E, F) UST_7 and UST_7_700; and (G, H) UST_XYZ and UST_XYZ_700. Afs, alkali-feldspar; Cal, Calcite; Cpx, Clinopyroxene; Hem, Hematite; I/S, mixed layers illite/smectite; Ilt, Illite; Pl, plagioclase; Qz, quartz.

aplastic inclusions. Coarse silt-sized particles (0.04–0.06 mm) are common, whereas the contents of very fine sand (0.06–0.125 mm), fine sand (0.125–0.25 mm), and medium sand (0.25–0.5 mm) vary widely, ranging from abundant to sporadic or rare. In contrast, coarse sand (0.5–1 mm) and very coarse sand (1–2 mm) fractions are consistently sporadic or rare. The overall relative abundance of aplastic inclusions (packing) ranges between 2% and 15% (area), with maximum grain sizes (MGS) ranging from 0.25 to 2.5 mm. Grain morphologies are predominantly angular to subangular, indicating very limited or no transport. Voids have irregular shapes and occupy just over 10% of the area. The micromass of the experimental briquettes fired at 700°C is generally optically active or, in some cases, slightly to fully inactive.

In terms of mineralogical and lithological composition, twinned plagioclase crystals constitute the dominant aplastic component, whereas alkaline feldspar is present sporadically. Opaque

TABLE 3 | Semi-quantitative results of the 28 Ustica samples with their mineralogical frequencies.

Sample code	Qz	Pl	Afs	Cpx	Ol	Cal	Amp	Hem	Ilt
UCRD_1	+++	+	+	tr	—	—	—	+	++
UCRD_2	+++	++	++/+	—	—	—	+	+	++/+
UCRD_3	+++	++	+	tr	tr	—	—	+/tr	++
UCRD_4	+++	++	+	+	tr	—	tr	+	++
UCRD_5	+++	++	++/+	tr	—	—	+	+	++/+
UCRD_6	+++	++	+	tr	—	—	tr	+	++/+
UCRD_7	+++	++	+	tr	tr	—	tr	+	++
UCRD_8	+++	++	++/+	tr	—	—	tr	+	++
UCRD_9	+++	++	+	+/tr	tr	—	—	+	+
UCRD_10	+++	++/+	+	+	+/tr	—	—	+	++/+
UCRD_11	+++	++/+	++/+	tr	—	+/tr	—	+/tr	++/+
UCRD_12	+++	++	+	—	tr	+/tr	—	+	++/+
UCRD_13	+++	++	++/+	—	—	—	+/tr	+	++
UCRD_14	+++	++	++	tr	—	+	—	+	+
UCRD_15	+++	++	++	—	—	+/tr	—	+	++
UCRD_16	+++	+	+++	tr	tr	++	tr	+/tr	++/+
UCRD_17	+++	++/+	+	tr	tr	—	—	+	++
UCRD_18	+++	++	+	—	—	+/tr	—	+	++
UCRD_21	+++	++	+	tr	—	—	—	+	++
UCRD_22	+++	++	++/+	tr	tr	—	tr	+	+
UCRD_23	+++	+	+	—	—	—	+	+	++
UCRD_24	+++	++	++	—	—	+/tr	tr	+	+
UCRD_25	+++	++	++/+	—	tr	—	—	+	++
UCRD_26	+++	++	+	tr	—	—	—	+	++/+
UCRD_27	+++	++	+	—	—	—	—	+	++
UCRD_28	+++	++	++/+	tr	tr	++/+	—	+	+
UCRD_29	+++	++	++	tr	tr	++	+/tr	+	++
UCRD_30	+++	++	+	+	+/tr	—	—	+	+

Note: Qualifiers legend: +++, abundant; ++, common; +, sporadic; tr, traces; —, not detected. Abbreviations: Afs, alkaline feldspar; Cc, calcite; Cpx, clinopyroxene; Hm, hematite.Ill + I/S, illite and mixed layer Illite/smectite; Pl, plagioclase; PML, pedogenic micrite lumps; Qz, quartz.

oxides range from sporadic to rare, and olivine, clinopyroxene, and amphibole occur as rare constituents. Rock fragments include common to rare basalts with intersertal or fluidal textures, as well as variably altered volcanic glass, which is also commonly present (Figure 6A–D). These characteristics are consistent across all samples, including UST_XYZ.

The main distinction lies in the presence of pedogenic microcrystalline calcite aggregates, which are abundant/common in UST_XYZ and sporadic in UST_4, but absent in the other fired clay samples (UST_5 and UST_7) (Figure 6E,F). Further details on the petrographic analysis of the experimental briquettes are provided in Table S2.

Relating to the chemical composition of clayey raw materials (Table S3), first of all, the difference between the UST_XYZ sample (Neolithic paleosol sampled in the Piano dei Cardoni excavation) and the other samples (UST_4, UST_5, and UST_7) in relation to the CaO concentration is striking. In fact, UST_XYZ is characterized by a CaO concentration equal to 10.35 wt.% (by weight), whereas in the other samples, it is much lower and varies from a minimum of 0.97 wt.% (UST_5) to a maximum of 3.39 wt.% (UST_4). These marked differences in the CaO content, considering that all the sampled soils (potential ceramic raw materials) derive from the weathering of volcanic products, find an obvious confirmation in the peculiarly widespread presence of lumps of microcrystalline calcite (micrite) already highlighted by microscopic observations. Concerning the other major elements' oxides, SiO_2 and Al_2O_3 have concentrations ranging, respectively, from 41.65 (sample UST_XYZ) to 53.71 wt.% (sample UST_4) and from 15.85 to 19.9 wt.% weight. Fe_2O_3 ranges from 6.35 to 8.66 wt.%, MgO ranges from 1.22 to 2.46 wt.%, Na_2O ranges from 1.05 to 1.81 wt.%, K_2O ranges from 1.61 to 2.37 wt.,% and TiO_2 ranges from 0.88 to 1.18 wt.% in weight. In terms of the SiO_2 values, these are higher in UST_4, characterized by a greater frequency of natural aplastic sand-sized granules (17 wt.% by weight), which are mostly composed of basaltic lithic fragments and glassy sherds. The relatively low magnesium concentrations likewise reflect the infrequent occurrence of ferromagnesian minerals (i.e., clinopyroxene, olivine, and amphibole), as seen

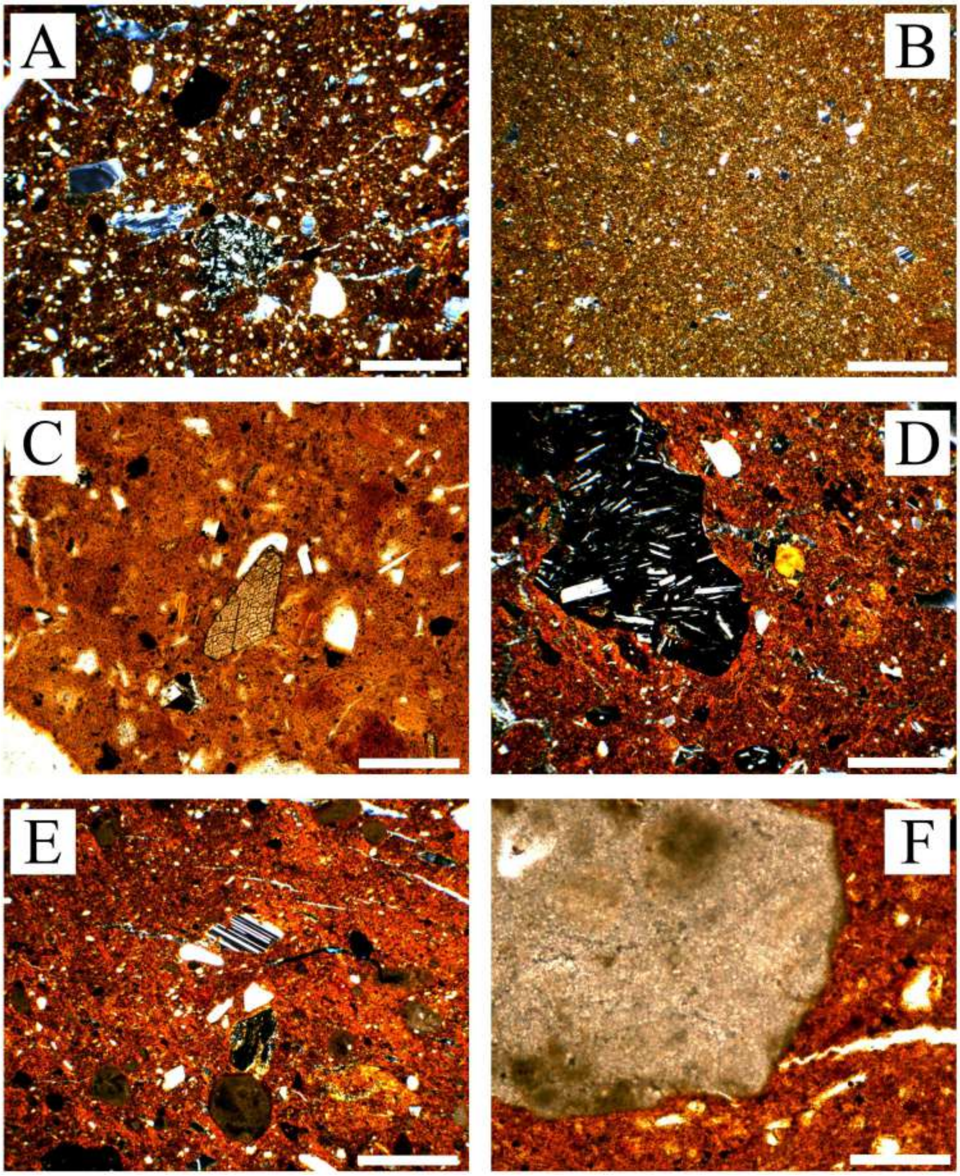

FIGURE 6 | Photomicrographs of clay firing tests (after firing at 700°C) under transmitted polarized light: (A) sample UST_4, plagioclase, alkaline feldspar, and basaltoid rocks fragments (XPL; scale bar = 0.5 mm). (B) Sample UST_5, with only a few small twinned plagioclase crystals scattered in the clayey-silty–sized groundmass (XPL; scale bar = 0.5 mm). (C) Sample UST_7, hornblende prismatic basal sections, with two cleavages, showing green pleochroism (PPL; scale bar = 0.1 mm). (D) Sample UST_7, a large basaltoid rock fragment surrounded by an optically active iron-rich groundmass (XPL; scale bar = 0.5 mm). (E) Sample UST_XYZ, several subregular and irregular pedogenic micrite lumps and twinned plagioclase crystal surrounded by an optically active groundmass (XPL; scale bar = 0.5 mm). (F) Sample UST_XYZ, view at higher magnification of the reaction rim between a pedogenic micrite lump and a clayey-silty–sized groundmass (XPL; scale bar = 0.1 mm).

after polarizing microscope observations. The high Na_2O content might be attributed to the plagioclase crystals (twinned and even millimetric in size), which, according to the microscopic examinations, prevail over the other monomineralic aplastic inclusions, especially compared to the values normally found in clayey raw materials with sedimentary origin. Furthermore, to justify the abundance of sodium in the soils of the small island of Ustica, the contribution due to the deposition of marine aerosols, also through rain and mist, could also be considered. In terms of the geochemically most significant trace elements, mainly in relation to the mineralogical compositions of the aplastic inclusions, a substantial homogeneity has been noted, even if with some significant variations. The concentrations of Ba, for example, are quite similar in the 4 samples analyzed, varying, respectively, from a minimum of 536 ppm (sample UST_4) to a maximum of 723 ppm (sample UST_XYZ). Slight variations within samples were also found for Sr, rare earths, Y, Th, and Nb. Only for the concentrations of Zr and Rb is the UST_5 sample (the only one with 2 wt.% by weight of sand-sized aplastic inclusions) significantly higher than all the others, equal to 307 and 128 ppm, respectively.

5.1.4 | *SEM-EDS Analysis of Unfired and Fired Tests (Briquettes)*

SEM-EDS analysis provided further insights into the mineralogical composition and microtextural features of the experimental briquettes, both unfired and fired at 700°C, including the degree of micromass sintering and the presence of secondary pores resulting from the firing process (Figure 7). It was observed that the microstructure of the groundmass changed only minimally after heat treatment at 700°C in an oxidizing atmosphere. This indicates that the firing temperature did not induce significant alterations, apart from the collapse of the crystalline structure of some clay minerals (illite, in particular, appears to be unaffected). EDS microanalysis confirmed the mineralogical composition of the aplastic inclusions previously identified by XRPD and optical microscopy. The main inclusions consist of volcanic glass fragments, which are either nearly pure (showing only Si and Al signals) or show evidence of argillification, with clay flakes containing iron and titanium oxide nanoparticles. Plagioclase and alkaline feldspar (common euhedral and subhedral crystals) were confirmed as abundant to common constituents, whereas femic minerals such as clinopyroxene, olivine, and amphibole were less frequent. Apatite, not detected via optical microscopy, was identified as an accessory mineral, typically occurring as very small anhedral crystals (5–20 μm), embedded in a ferruginous clay matrix.

Iron-rich clay pellets were also identified morphologically and compositionally through secondary electron imaging and EDS point analysis, likely resulting from incomplete processing of the clay paste during briquette preparation. Microcrystalline calcite lumps, mostly between 0.1 and 1 mm in size, were abundant in sample UST_XYZ, with their composition verified by EDS through elevated calcium concentrations. No microtextural evidence of sintering or vitrification was observed in any of the fired specimens. Even in sample UST_XYZ, despite the presence of common micrite lumps, no sintered ones with amygdaloid secondary pores were detected (Figure 7H).

5.2 | Ceramics

5.2.1 | XRPD Analysis

The evaluation of the patterns obtained by the XRPD analysis on the ceramic samples allowed their division into classes according to their bulk mineralogical composition. The first class, matching to approximately 30% of the total samples (9 of 28), is characterized by the presence of calcite (samples UCRD_11, 12, 14, 15, 16, 18, 24, 28, and 29). In this class, calcite can be present in quantities widely varying from common to sporadic/rare (Figure 8A). The second class, which includes the majority of the ceramic finds analyzed (about 70%), on the contrary, is characterized by the absence of calcite (Figure 8B). In both classes, quartz and plagioclase are the prevalent crystalline phases, showing the most intense reflections. Finally, the mineralogical association that represents the first ceramic class, in decreasing order of abundance, is as follows: quartz + plagioclase + alkaline feldspar + calcite + illite ± hematite, whereas for the second one, it is as follows: quartz + plagioclase + alkaline feldspar + illite ± hematite. Clinopyroxene, olivine, and amphibole were only sporadically detected in both the considered "mineralogical classes" and always in trace quantities.

5.2.2 | Petrography and Chemistry

The petrographic characterization of the new 28 ceramic samples from recent excavations at Piano dei Cardoni has enabled the refinement and expansion of previous observations concerning the compositional and textural attributes of locally produced Neolithic pottery (Speciale, Montana, et al. 2021). This advancement stems not only from the increased number of thin-section analyses (building on the 30 samples previously described; Speciale, Montana, et al. 2021) but also from new data obtained through minero-petrographic analysis of experimentally fired briquettes prepared from local clay raw materials. Polarized light microscopy and XRPD analyses reveal that approximately 30% of the ceramics contain pedogenic microcrystalline calcite lumps, allowing discrimination of two principal petrographic fabric groups. The first group (nine samples: UCRD_11, 12, 14, 15, 16, 18, 24, 28, and 29; Table S2) features sporadic to common calcite lumps (Figure 9A,B), whereas the second group (UCRD_1, 2, 3, 4, 5, 6, 7, 8, 9, 10, 13, 17, 21, 22, 23, 25, 26, 27, and 30) lacks these features. The presence of microcrystalline calcite in the Neolithic paleosol sample (UST_XYZ) from Piano dei Cardoni supports the interpretation that these calcite lumps in ceramics derive from local pedogenic inputs. Variability within each group is mainly linked to differences in larger lithic aplastic inclusions, which are predominantly basaltic fragments and, in some instances, trachytoid fragments (e.g., UCRD_2, 5, 13, 16, 22, and 28). Despite this mineralogical–petrographic distinction, both fabric groups share compositional and textural characteristics strongly indicative of local manufacture. All samples contain variable amounts of altered volcanic vitreous scoriae and irregularly shaped clayey–ferruginous aggregates, the latter particularly abundant in UCRD_2, 6, and 8. Textural analysis shows a heterogeneous distribution and serial sorting of aplastic inclusions, dominated by coarse silt (0.04–0.06 mm) and very fine sand (0.06–0.125 mm). Medium sand (0.25–0.5 mm) abundance varies from common to rare, whereas coarse (0.5–1 mm) and very coarse sand (1–2 mm) are sporadic to rare. Aplastic inclusion packing ranges broadly between 5% and 20% area, with maximum grain sizes ranging from 0.3 to 2.2 mm. Granule morphology is predominantly angular or subangular, rarely subrounded.

Macroporosity (pore diameter of a few micron) ranges from 5% to 20%, with pores manifesting as channels, planar voids, and vugs.

Mineralogically, plagioclase and alkali feldspar monocrystals dominate the aplastic fraction, with common subspherical opaque oxides. Accessory components such as olivine, clinopyroxene, and amphibole are sporadic or rare. Rock fragments primarily include basalts with intersertal to fluidal textures and variably altered volcanic glass (scoriae), some containing glomerophyric plagioclase (Figure 9C–F). Trachytic lavas are also present in certain samples.

Optical activity of the micromass is generally medium to high, corroborated by XRPD and SEM-EDS data, indicating firing temperatures around or slightly exceeding 700°C (Maggetti et al. 2011).

Microscopic examination under plane polarized light (PPL) reveals clay-based coatings on several ceramic bodies (e.g., UCRD_1, 3, 16, 21, and 25–29), ranging from 100 to 200 μm in thickness, often serving as preparatory layers for painted decoration. Iron oxide–based paints are thinner (< 30 μm). Two distinct engobe types are identified: one comprising decanted clay purified of coarse sand, but containing abundant small

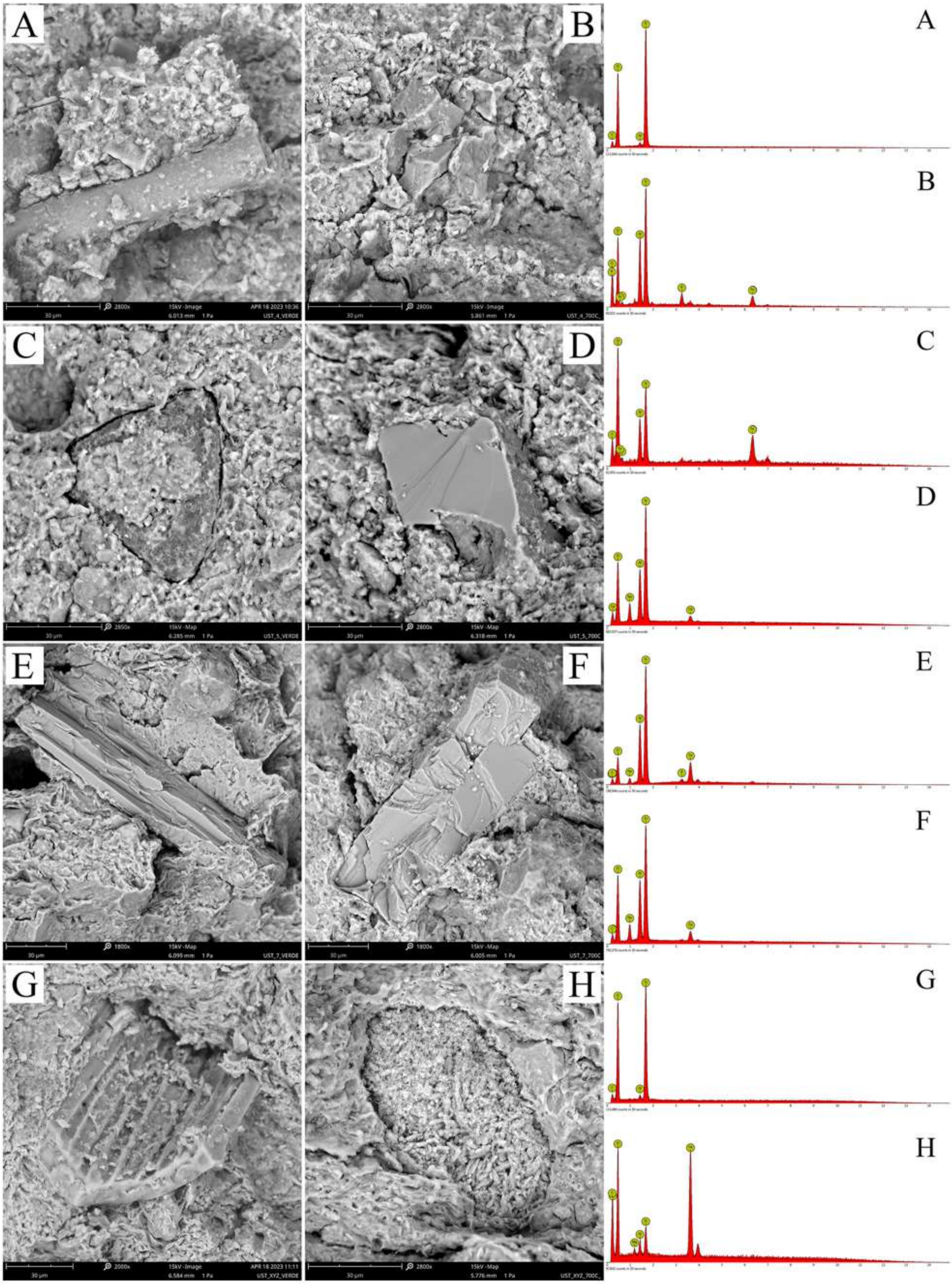

FIGURE 7 | Legend on next page.

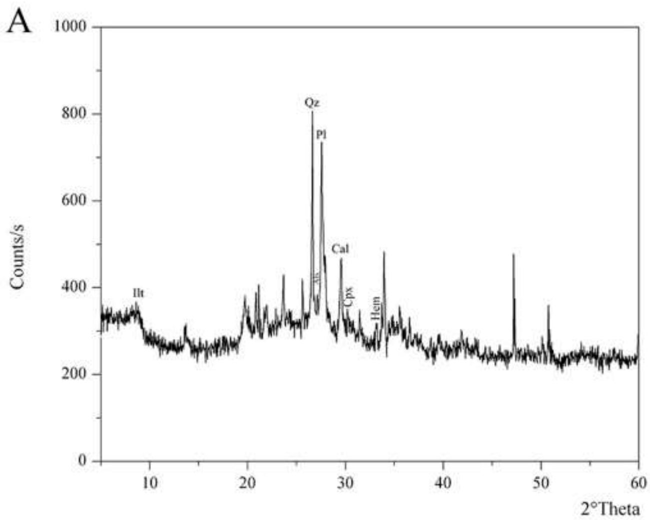

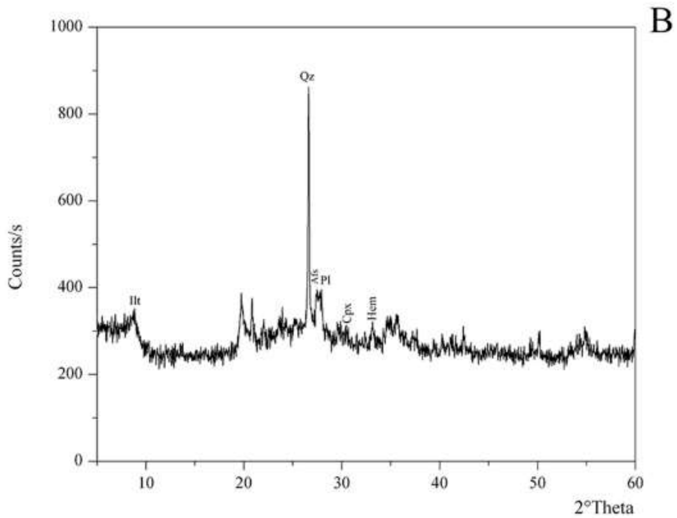

FIGURE 8 | Representative XRPD patterns of the two main mineralogical classes identified in the studied ceramic assemblage. (A) Calcite bearing mineralogical class (sample UCRD_16). (B) Calcite poor mineralogical class (sample UCRD_23). Afs, alkali-feldspar; Cal, Calcite; Cpx, Clinopyroxene; Hem, Hematite; Ilt, Illite; Pl, plagioclase; Qz, quartz.

micrite lumps (20–40 μm), and another composed of iron oxide–rich clay without micrite lumps (Figure 10).

For the chemical analyses (ICP-OES + ICP-MS), approximately 50% of the ceramic samples were selected (13 out of 28). Table S3 shows all the results regarding both the ceramic finds and the local raw materials (55 analyzed, including major, minor, and trace elements). Regarding the major elements, it is immediately evident that the samples showing common to sporadic/rare pedogenic micrite lumps during the polarizing microscope observation (only UCRD_11, 12, 16, 24, and 28 were selected for chemical analysis) are characterized by relatively higher CaO concentrations varying from 2.85 wt.% up to 5.04 wt.% (average 3.62 wt.%) compared to ceramic samples in which pedogenic micrite lumps had not been found. The latter (only UCRD_1, 2, 5, 6, 7, 22, 25, and 26 were selected for chemical analysis), nevertheless, show CaO values that vary from a minimum of 2.00 wt.% up to a maximum of 2.62 wt.% (average 2.42 wt.%), which are, on average, up to 40 wt.% lower than the finds with variable quantities of pedogenic micrite lumps (Table S1A,B). No relevant chemical differences in the concentration of all the major and minor elements can be observed between the two chemical subgroups, defined on the basis of the average concentration of CaO and corresponding to the two petrographic subgroups (presence or absence of pedogenic micrite lumps). In fact, the average values of these elements are well comparable and similar between the two subgroups. Moreover, the relative standard deviations (RDS) are always reasonably low (generally well below 10%). The only exceptions are MnO, Na_2O, and P_2O_5 concentrations. Manganese and sodium (expressed as oxides) are characterized by a rather higher variability (RDS even higher than 20%). Nevertheless, they show very similar average values in the two subgroups.

In contrast, P_2O_5 is notably more concentrated in the ceramic samples that lack pedogenic micrite lumps. Regarding trace elements, the average values between the chemical subgroups described above are generally consistent. The only notable exception is barium (Ba), which constantly shows slightly higher concentrations—approximately 25% more—in the ceramics without pedogenic micritic calcite (average 1250 ppm), compared to those that contain it (average 938 ppm). Once again, the RDSs for trace elements are quite low, mostly below 20% and sometimes even close to or less than 10% (i.e., Zr, La, and Ce), suggesting good chemical homogeneity of the ceramic produced in Ustica during the Neolithic.

5.2.3 | *Scanning Electron Microscope (SEM)*

SEM-EDS analysis provided detailed insights into the microfabric of the ceramic samples, offering valuable evidence for reconstructing the ceramic production technology practiced on the island of Ustica during Neolithic. Consistent with previous studies, most ceramic fabrics were produced using non-calcareous, ferriferous clay raw materials (Tite and Maniatis 1975). Consequently, the firing temperatures were likely relatively low—around or below 700°C—insufficient to trigger significant morphological transformations in the groundmass particles via sintering processes (Figure 11). This interpretation is supported by the absence of vitrification features (NV) in all samples, consistent with the findings of Maniatis and Tite (1981).

FIGURE 7 | Clay firing tests observed at SEM-EDS: (A) sample UST_4 (unfired), volcanic glass sherd surrounded by the groundmass (see the EDS spectrum). (B) Sample UST_4 (fired at 700°C) altered alkaline feldspar in the iron-rich groundmass (see the EDS spectrum). (C) Sample UST_5 (unfired), iron-rich lump (see the EDS spectrum). (D) Sample UST_5 (fired at 700°C) anhedral plagioclase in the groundmass (see the EDS spectrum). (E) Sample UST_7 (unfired), euhedral plagioclase crystal (see the EDS spectrum). (F) Sample UST_7 (fired at 700°C), subhedral plagioclase crystal (see the EDS spectrum). (G) Sample UST_XYZ (unfired), volcanic glass fragment in groundmass (see the EDS spectrum). (H) Sample UST_XYZ (fired at 700°C), pedogenic microcrystalline calcite lump (see the EDS spectrum).

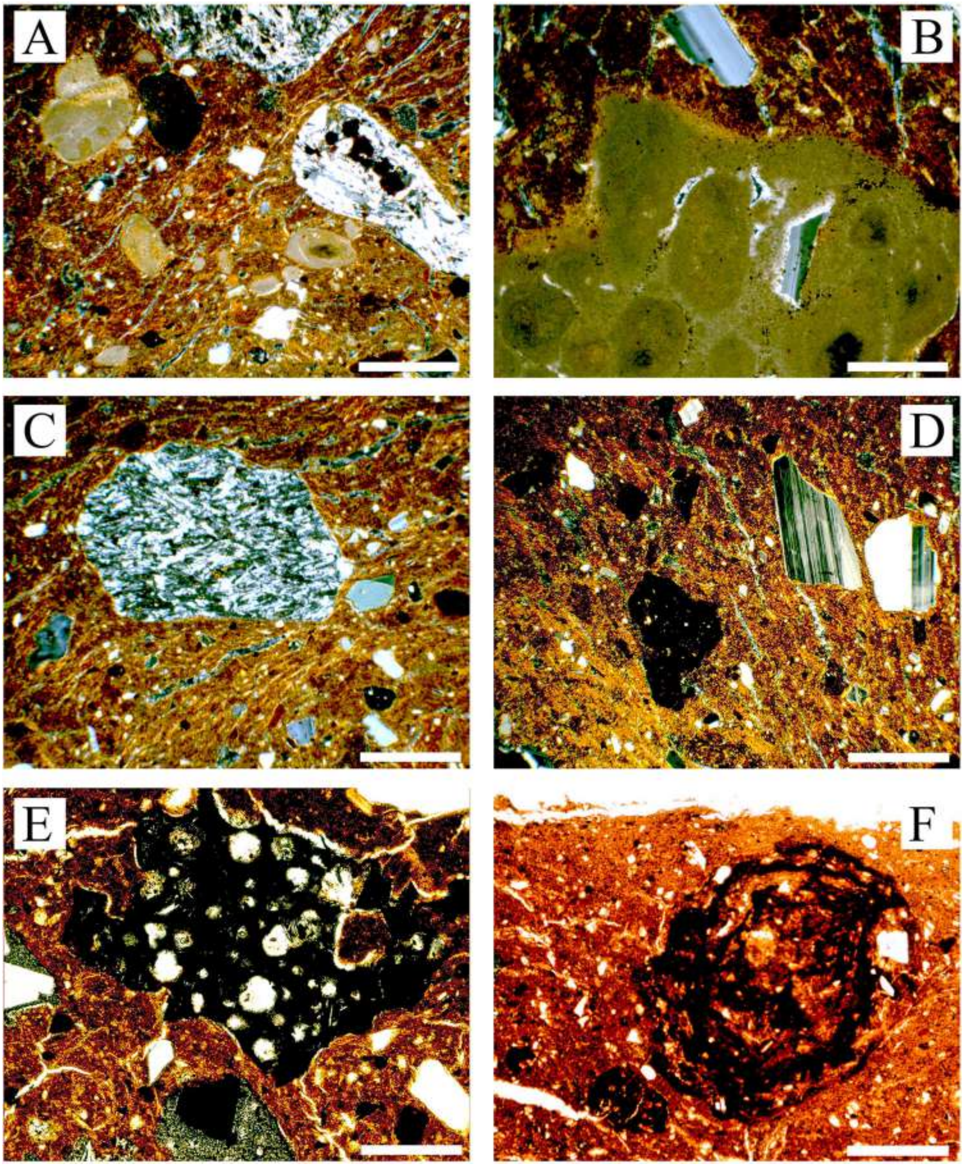

FIGURE 9 | Thin-section photomicrographs showing some peculiar compositional and textural features of the ceramic samples: (A) sample UCRD_16, overview of the groundmass characterized by several submillimetric (mostly under 0.5 mm) pedogenic micrite lumps and volcanic aplastic grains (XPL; scale bar = 0.5 mm). (B) Sample UCRD_16, detail of a pedogenic micrite lump showing a concretionary/orbicular texture, which, during its development, incorporated a tiny plagioclase crystal (XPL; scale bar = 0.2 mm). (C) Sample UCRD_2, subangular millimetric trachytoid lithic fragment (XPL; scale bar = 0.5 mm). (D) Sample UCRD_3, clear and little altered plagioclase crystals with small, angular, and little vesicular glassy scoriae (XPL; scale bar = 0.5 mm). (E) Sample UCRD_28, detail of a well-vesicled volcanic glassy scoria (PPL; scale bar = 0.2 mm). (F) Sample UCRD_4, subcircular lump rich in iron oxides (PPL; scale bar = 0.2 mm).

In samples containing pedogenic microcrystalline calcite lumps, the lack of reaction rims or secondary calcite phases as well as no signs of thermal alteration further support firing temperatures below the decomposition threshold of $CaCO_3$. This interpretation is reinforced by experimental firing of the UST_XYZ' Neolithic paleosol sample from Piano dei Cardoni at a controlled temperature of 700°C. It is well established that the thermal decomposition of calcite into calcium oxide proceeds gradually and accelerates only at temperatures above approximately 750°C (Karunadasa et al. 2019). Consistently, XRPD analyses of the ceramic samples revealed no evidence of secondary mineral phases such as calcium silicates—gehlenite and wollastonite—which typically form at temperatures exceeding 800°C and 900°C, respectively (Gliozzo 2020).

SEM-EDS analysis also facilitated the characterization of both the composition and morphology of the dominant monomineralic inclusions, which include alkali-feldspar, plagioclase, and lithic fragments derived from basalt, trachyte, and volcanic glass scoriae (Figure 11A,B). Post-firing morphological details of the pedogenic micrite lumps were also documented. Their outer edges showed no signs of reaction with the surrounding aluminosilicate groundmass, likely reflecting the relatively low firing temperatures. In the sample URCD_16, calcite crystals forming the micrite lumps predominantly measure 1–10 μm and show euhedral (scalenohedral) or subhedral crystal habits (Figure 11C).

Some micrite lumps incorporated variable amounts of clay matrix and iron oxides/hydroxides. For instance, EDS spot analyses of lumps in sample UCRD_11 revealed compositional

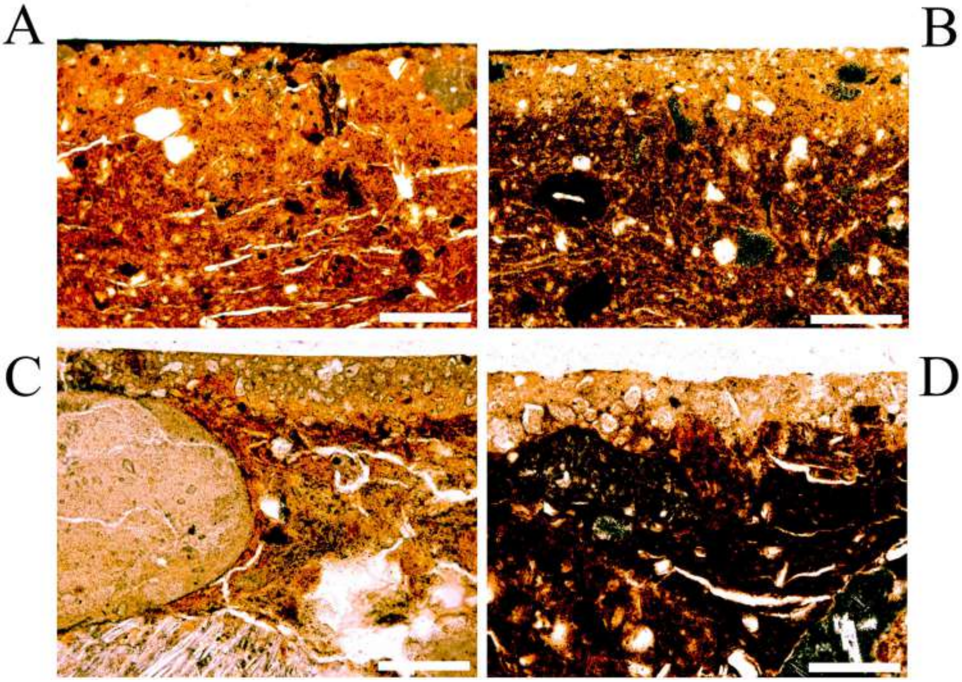

FIGURE 10 | Thin-section microphotographs of the coatings that cover the ceramic body: (A) sample UCRD_12 cross section, depurated clay-based coatings, rich in iron oxides and covered with a thin and irregular layer of black paint (XPL; scale bar = 0.5 mm). (B) Sample UCRD_25 cross section, depurated and iron oxide–rich clay-based coatings, irregularly covered with black paint (XPL; scale bar = 0.2 mm). (C) Sample UCRD_16 cross section and (D) sample UCRD_28 cross section, examples of clay coating layers deprived of the medium-coarse volcanic sandy fraction but characterized by numerous small pedogenic micrite lumps (XPL; scale bar = 0.5 mm).

heterogeneity, with calcite microaggregates interspersed with clay micelles. Variations in Ca concentrations corresponded to the relative abundance of clay minerals and iron oxides/hydroxides, as indicated by Si, Al, K, and Fe peaks in the EDS spectra (Figure 11D).

Calcium-rich, clay-based surface coatings (engobes) were identified through standardless EDS spot analysis in samples UCRD_7, 16, and 22 (Figure 11E). Notably, this method also revealed barite mineralization in sample UCRD_22 (Figure 11F).

6 | Discussion

In any territorial and chronological framework, a comprehensive understanding of ceramic production must encompass the entire operational chain, from raw material procurement and paste preparation to shaping and firing.

An in-depth characterization of ceramic artifacts alone is insufficient to fully unravel the complexities behind their manufacture or to assess the technological sophistication achieved by past communities. Instead, an integrated approach that includes the study of local raw materials availability and their compositional and textural features is essential. Such analyses provide a realistic basis for evaluating the technological knowledge developed within the settlement and for interpreting the functional and esthetic attributes of the ceramic assemblage. Moreover, this approach allows for meaningful comparisons with coeval cultural contexts.

Ustica, a volcanic island inhabited since the Neolithic, was occupied during a period of demographic expansion across Southern Italy and Sicily. The establishment of a permanent settlement at Piano dei Cardoni reflects broader Middle Neolithic socio-cultural transformations in the region. Archaeological evidence, including agricultural practices, craft production, and participation in exchange networks, indicates a complex social organization with specialized roles. Ustica's strategic maritime position likely enhanced its function as a node in regional trade routes, increasing its cultural and economic relevance during this period. The high occurrence of painted pottery (Magrì et al. 2023), alongside funerary practices (Speciale et al. 2024), suggests strong cultural connections between Ustica and mainland regions such as Apulia and Basilicata, home to the *Serra d'Alto* culture.

Local ceramic production in prehistoric Sicily and subsequent periods is well documented on other minor volcanic islands, including Lipari and Pantelleria. Ceramic manufactures with volcanic inclusions have also been proven in the surrounding area of the Etna volcano and in the Hyblaean territory (southeastern Sicily), although these ceramic fabrics are more frequently made from tertiary or quaternary marine sedimentary clays, typically with CaO contents exceeding 5 wt.%. In contrast, the Sicilian volcanic islands—formed between approximately 700,000 and 500,000 years ago—feature clays of hydrothermal origin (Lipari and Pantelleria) or pedogenically altered volcanic materials (Ustica). Pedogenetic processes acting on eruptive products, including lavas and pyroclastics, promote the transformation of primary minerals and volcanic glass into clay minerals through oxidation, dissolution, and hydrolysis (Mirabella et al. 2005). Consequently, clays derived from the weathering of volcanic deposits commonly contain intimately mixed hydrated and weakly crystalline iron oxides.

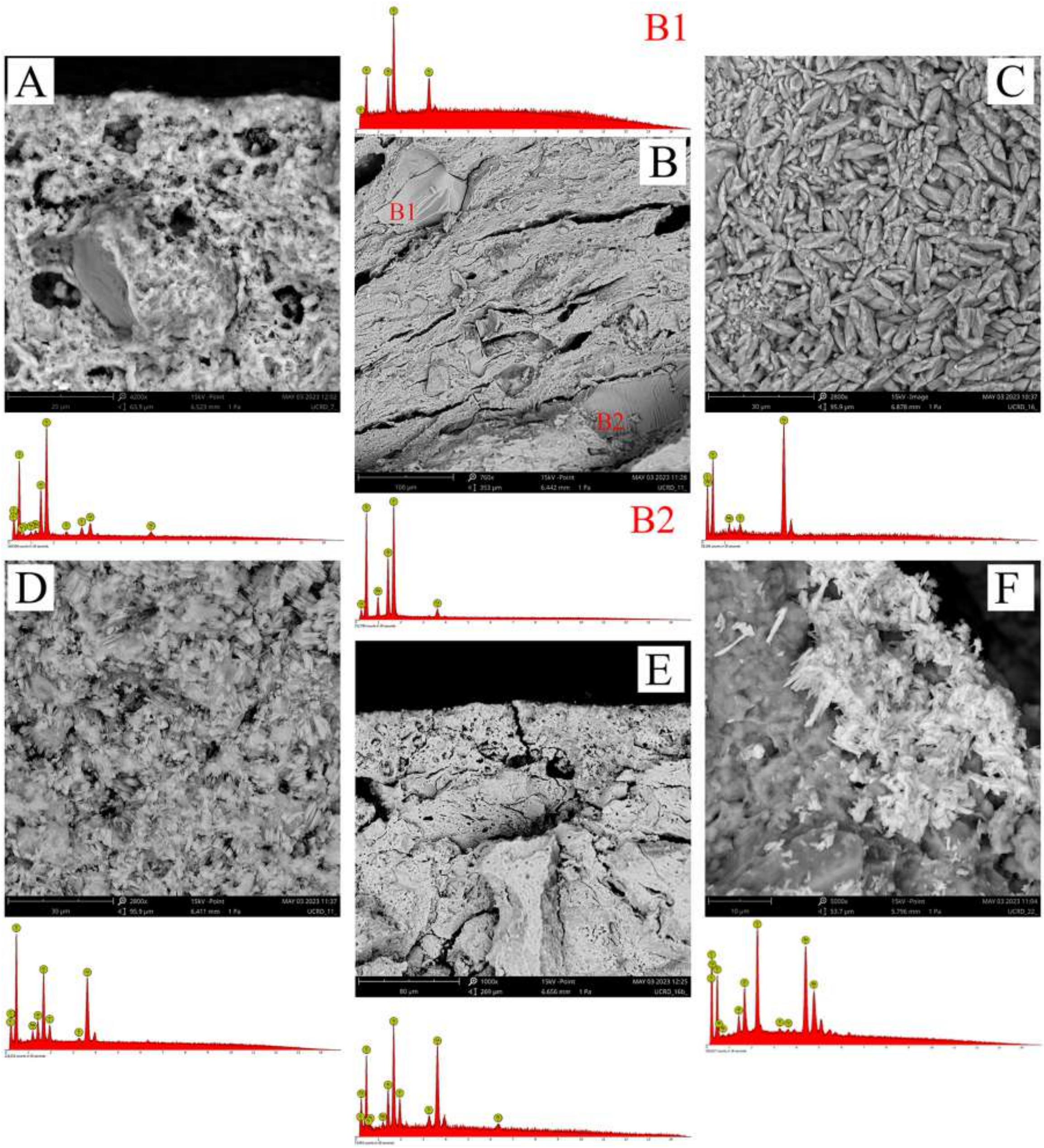

FIGURE 11 | SEM images (BSEI) and corresponding EDS compositional spectra (spot analysis): (A) sample UCRD_7, overall image of the groundmass with glassy scoriae or monomineralic aplastic inclusions and corresponding qualitative chemical analysis (EDS spectrum). (B) Sample UCRD_11, two monomineralic aplastic inclusions: alkali feldspar (EDS spot B1) and plagioclase (EDS spot B2). (C) Sample UCRD_16, morphological details and EDS spectrum of a pedogenic micrite clot in which the subhedral (scalenohedral) morphology of most of the calcite microcrystals can be observed. (D) Sample UCRD_11, pedogenic clot in which calcite and clay particles are mixed, as highlighted by the corresponding EDS spectrum. (E) Sample UCRD_28, detail of the purified clay coating layer and corresponding EDS analysis. (F) Sample UCRD_22, aggregate of minute barium sulfate (Barite) crystals characterized by a high back-scattering coefficient in the edges of a pore.

Geologically, each colluvial or alluvial deposit on a volcanic island reflects the unique lithological composition of its dominant eruptive products. These compositional signatures serve as markers, enabling differentiation between ceramic productions. Textural characteristics of natural raw materials—such as the abundance and size distribution of aplastic inclusions within the sand fraction, and the relative proportions of sand, coarse silt, fine silt, and plastic clay—offer additional clues for tracing raw material sources and inferring artisans' technical expertise. The ceramic samples analyzed here fully conform to the minero-petrographic profile previously established for ceramics from Piano dei Cardoni (Speciale, Montana, et al. 2021), and are consistent with magmatic products outcropping on Ustica (Cinque et al. 1988; de Vita et al. 1998; Peccerillo 2005). Under the polarizing microscope, these local ceramics are readily distinguishable from Neolithic and Bronze age productions from Lipari (Aeolian Islands) and Pantelleria, which show different mineralogical and lithic assemblages. Lipari fabrics contain intermediate to acidic volcanic rock fragments, such as andesite basalts, rhyolites, pumices, obsidian shards, zoned plagioclase, Carlsbad twinned sanidine, and abundant femic minerals (mainly clinopyroxene), reflecting the calc-alkaline typical of the Aeolian islands (Williams 1980; Williams and Levi 2008; Brunelli et al. 2013; Levi et al. 2020). Similarly, Pantelleria ceramics differ markedly, containing lithics and monomineralic grains typical of sodium-rich peralkaline volcanism, including pantellerite (Na-peralkaline rhyolite), pantelleritic trachytes, vesiculated iron-rich basaltic scoriae and pumices, predominant alkali feldspar (anorthoclase), primary quartz, green clinopyroxene (aegirine-augite), and the rare deep red aenigmatite (Montana et al. 2007).

Considering the raw materials suitable for ceramic production on Ustica, the experimental briquettes fabricated from local clayey colluvial deposits provide valuable insights. Notably, half of the briquettes—specifically UST_5 and UST_7—show mineralogical and chemical compositions closely matching the ceramic petrochemical group characterized by the absence of pedogenic micrite lumps, which represents nearly 70% of the analyzed archaeological ceramics. Conversely, the briquettes made from UST_4 and particularly UST_XYZ show textural and compositional features consistent with the ceramic group containing sporadic to common pedogenic micrite lumps, which constitute about 30% of the total ceramic assemblage.

The presence of micrite lumps (subrounded to irregular shapes, mostly between 0.2 and 1 mm) in the raw materials (notably in UST_XYZ and to a lesser extent UST_4), and their persistence after firing at 700°C in an oxidizing atmosphere—showing minimal alteration aside from some iron oxide segregation—provides strong evidence that these features are original components in a subset of the Neolithic ceramics from Piano dei Cardoni. This underscores the critical role of experimental firing of potential raw materials as a baseline for comparison with archaeological finds.

Importantly, micrite lumps of this size could otherwise be misinterpreted as deliberately added temper to enhance ceramic performance, or attributed to vague ritualistic purposes, or alternatively considered secondary deposits resulting from post-depositional burial processes. However, the experimental results support the interpretation that these micrite lumps are intrinsic inclusions in the raw material rather than later additions.

XRPD analyses further confirm that the experimental briquettes share similar mineralogical assemblages with local Neolithic ceramics. Quartz, present in all briquettes and ceramic samples, likely originates from the silty fraction of local clays and remains stable up to 1100°C (El Ouahabi et al. 2015).

Illite is also consistently detected and is known to persist up to approximately 950°C, with its gradual decomposition beginning near this temperature (Peters and Iberg 1978).

The presence or crystallization of hematite at 700°C can be attributed to iron oxides and hydroxides originally present in the unfired clay, which become more crystalline upon firing. For the group containing micrite lumps, calcite remains stable at 700°C in the experimental briquettes but is known to decompose at temperatures exceeding 800°C (Cultrone et al. 2001).

Moreover, a number of consistent similarities were observed across all analyzed ceramic raw materials, not only in terms of texture and mineralogical/lithological composition but also regarding their groundmass characteristics. Clay pellets occur with a prevalent to sporadic frequency, suggesting incomplete or insufficient clay mixing during paste preparation. Some pellets appear black with sharp, well-defined boundaries, whereas others are brown with more diffuse, merging rims. The black coloration correlates with a higher concentration of Fe(II) oxide (FeO) within the pellets, contrasting with the Fe(III) oxide (Fe_2O_3) concentration in the surrounding groundmass. Microcrystalline calcite was also identified in both categories of samples.

The mineralogical composition of inclusions, especially lithic fragments found in the experimental briquettes, reflects the diverse geology surrounding the sampling locations on Ustica Island. These include subaerial basaltic lavas from Monte Guardia dei Turchi, mugearite lava flows from Gorgo Salato, lava-block terraced deposits from Piano dei Cardoni, palagonite and hyaloclastic breccias of the Spalmatore Formation in Cala Sidoti, and submarine lavas at Punta San Paolo. The lithic fragments detected in the ceramics correspond closely with these local geological formations. For example, the Punta Spalmatore area (western Ustica) comprises palagonite and hyaloclastic breccias, whereas Grotta Azzurra and Grotta San Francesco (eastern Ustica) display sub-alkali basaltic pillow lavas and hyaloclastite. Cala di Santa Maria contains submarine lavas and breccias adjacent to mugearite flows, and the Rocca della Falconiera area features a stratified tuff cone in the eastern sector. Additionally, subaerial basaltic lavas are present at Monte Guardia dei Turchi and trachytic lithics occur at Grotte del Lapillo, associated with pumice-fall layers and lag breccias. Pedogenic lava-block terraced deposits at Piano dei Cardoni represent glacio-eustatic sea-level fluctuations during the Middle to Upper Pleistocene (de Vita 1993; de Vita et al. 1998; Bonomo and Ricci 2010; Furlani et al. 2017; de Vita and Foresta Martin 2017; Foresta Martin and Furlani 2021).

The identification of volcanic rock types (basalts vs. trachytes) under the microscope principally relies on the plagioclase to alkali-feldspar ratio within the groundmass. Hence, ceramic fragments can be sub-grouped based on the sporadic presence of trachytic lithics, whereas others contain exclusively basaltic shards. However, these variations appear to be random rather than the result of deliberate artisan selection aimed at achieving specific functional properties.

Regarding the optical activity of the groundmass, it generally ranges from highly to slightly active, which aligns with firing temperatures estimated at around 700°C. Samples with a light core with darker rims likely reflect firing conditions that shifted from oxidizing to reducing atmospheres—oxygen penetrated sufficiently to oxidize the ceramic core, whereas the rims remained less oxidized (Quinn 2013). Finally, the absence of bimodal particle size distribution in the ancient ceramics suggests that raw clayey materials were used with minimal or no added temper.

Considering the overall petrochemical characteristics, the ancient ceramics show a clear association with the fired contemporary clayey raw materials, as evidenced by the close similarity in their microfabrics. Specifically, the first group of Neolithic ceramics corresponds to the experimental briquettes lacking microcrystalline calcite (UST_5 and UST_7). In contrast, the second group aligns with the fired clays containing secondary calcite (UST_XYZ and UST_4). The presence of micrite lumps within the clayey soil strongly supports the interpretation that calcite was an original component of the raw material rather than a product of secondary deposition during post-depositional burial processes.

This petrographic correlation between the archaeological ceramic samples and the experimentally fired clays reinforces the conclusion that ceramic production was local but involved raw materials sourced from different extraction sites, all sharing the same fundamental lithological characteristics, namely, basaltic and/or of trachytic bedrocks.

Chemical analyses further support this linkage. A key chemical marker is the CaO concentration, which distinguishes both ceramics and raw materials. Ceramic samples containing micrite lumps show CaO contents ranging from 2.85 to 5.04 wt.% (mean 3.62 wt.%), whereas those without micrite lumps have lower values between 2.0 and 2.62 wt.% (mean 2.42 wt.%). Similarly, CaO concentrations in the raw materials are low for UST_5 and UST_7 (~ 1.9 wt.%) but markedly higher in UST_4 (3.87 wt.%) and especially UST_XYZ (12.84 wt.%), paralleling the ceramics with varying amounts of micrite lumps (from rare to common).

This compositional matching between the two ceramic groups and the local clay deposits (Belfiore et al. 2022; Di Bella et al. 2019) can be effectively visualized through scatter diagrams of elemental concentration ranges (Figure 12). From an archaeological perspective, these findings suggest that ceramic objects such as UCRD_11, 12, 14, 15, 16, 18, 24, 28, and 29 were likely manufactured using clays sourced directly from the Piano dei Cardoni area. Conversely, other ceramic finds appear to derive from clay deposits located between the southern slopes of Monte Guardia dei Turchi and Gorgo Salato, near the Bronze Age settlement.

SEM-EDS analysis, comparing the experimental briquettes with archaeological ceramics, confirmed the presence of Fe-rich clay lumps randomly dispersed within the ceramic groundmass as well as pedogenic microcrystalline calcite lumps. In particular, sample UCRD_22 revealed barite ($BaSO_4$) as a secondary, likely burial-related phase. This is consistent with the very low solubility of barium sulfate (0.0024 g/L at 25°C), which promotes its precipitation. Geochemically, Ba is closely linked to potassium and thus relatively abundant in feldspars; it can be mobilized during surface weathering through alkaline hydrolysis of the magmatic source rocks.

Notably, no significant microstructural differences emerged between unfired and fired clay materials. The firing temperature used for the experimental briquettes (700°C) was low enough to prevent notable textural or ultrastructural changes, resulting in a microstructure closely resembling that of the unfired raw material. This is mainly due to the low CaO content in these clays, which inhibits vitrification or the formation of secondary porosity typically associated with calcareous clays fired above 800°C. As a result, no new crystalline mineral phases were detected, and the overall microstructure remained consistent.

The comparative mineralogical and SEM-EDS data further suggest that the archaeological ceramics and experimental briquettes were fired at similarly moderate temperatures, likely at around 700°C, rather than at higher firing temperatures.

SEM-EDS also provided insights into the surface treatments and finishes of the ceramics. Lighter reddish surfaces showed ocher pigments applied over clay preparations relatively richer in small silty $CaCO_3$ lumps (Figure 11D). Conversely, darker reddish to blackish-brown surfaces rested on clay matrices richer in iron (Figure 11F). These observations imply deliberate raw material selection tailored to desired firing outcomes and surface esthetics, reflecting detailed knowledge of the local geomaterials available near the settlement and elsewhere on Ustica. Such choices underscore a sophisticated technical understanding of the manufacturing phases.

Integration of these archaeometric findings with macroscopic and technological observations raises the question of whether the two petrographic fabric groups identified—those (A) lacking and those (B) containing microcrystalline calcite lumps—correspond to specific vessel types, either functionally or in terms of surface treatment.

A thorough review of the 28 ceramic samples showed no clear or consistent distribution patterns between these two groups. Samples without micrite (Table S1A) were found across a variety of vessel forms, including both small, finely crafted tableware (figs. 2.7–10, 12) and larger, coarse storage or processing vessels with thicker walls and roughly smoothed surfaces (figs. 2.1, 3–6).

The same homogeneous distribution is observed regarding surface treatments, as no exclusive or consistent correlation can be established among the groups of smoothed, burnished, and painted wares. Similarly, the samples containing micrite lumps (Table S1B) show a non-specific distribution; however, there is a slight predominance of red-on-white painted vessels within this group (six out of nine samples) (fig. 2.2, 11). Notably, all ceramic specimens from Trench 3 (10 out of 28 samples) lack microcrystalline calcite lumps, possibly indicating the preferential use of locally available with sporadic or absent pedogenic micrite, sourced from areas not immediately adjacent to the funerary structure (fig. 2.1).

The discussion becomes more compelling when focusing on vessel surface finishing and decoration.

Microscopic analysis in plane polarized light (PPL), combined with SEM-EDS observations, has identified two distinct types of clay-based "engobes" or preparatory coatings applied for surface treatment:

1. A light-colored coating derived from decanted clay containing small micrite lumps, primarily associated with vessels featuring red painted decoration on a white background.
2. A reddish to darker engobe, enriched in iron oxides, observed on specimens with red or red-brown burnished surfaces.

This differentiation is significant, as it not only reveals the Neolithic community at Piano dei Cardoni's in-depth technical knowledge and response to the raw materials available locally but also a deliberate pursuit of specific "recipes" aimed at achieving distinct esthetic effects on the vessels.

The presence of different coating types is particularly noteworthy for describing the unique red-banded painted ware, a distinctive category within the Piano dei Cardoni assemblage (e.g., UCRD_16, 21, and 28; figs. 2.8, 11, and 14), and offers

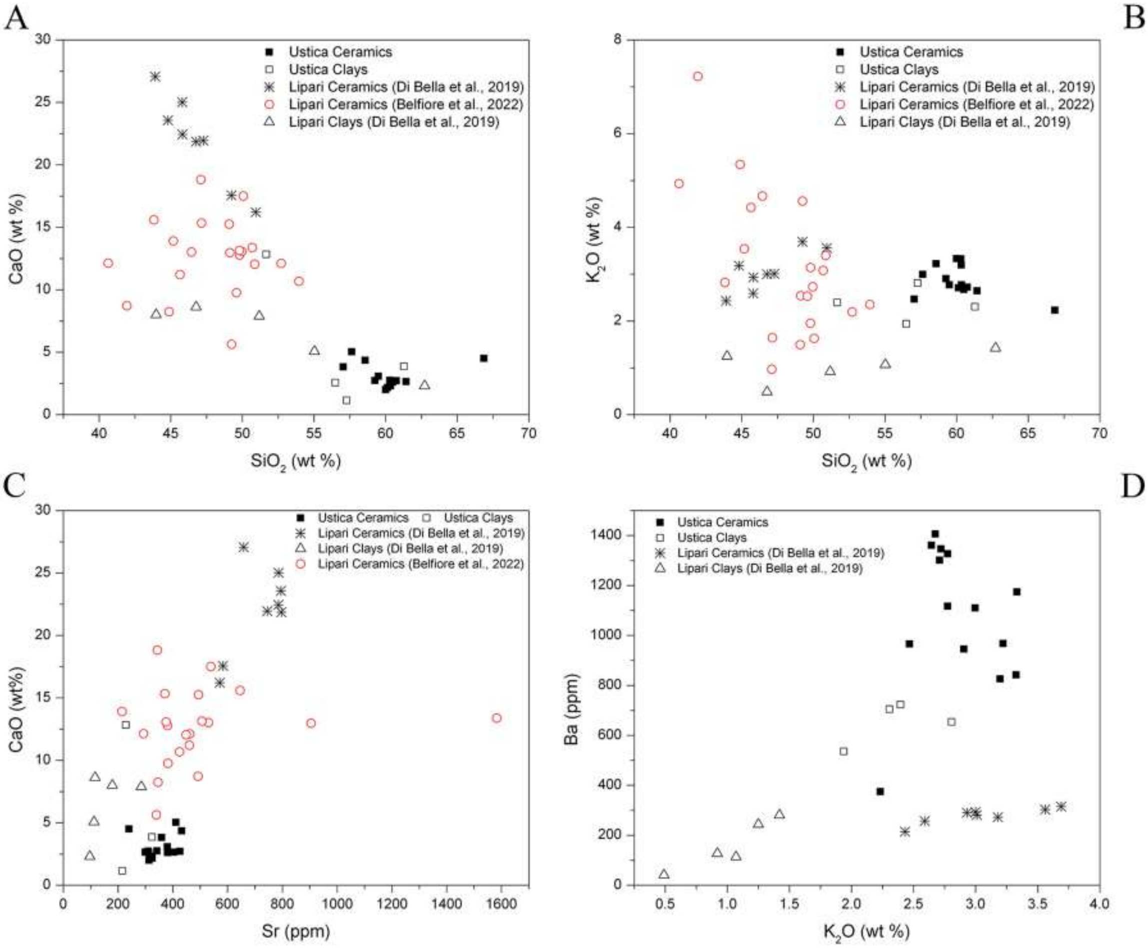

FIGURE 12 | Comparison based on the concentration of some major and trace elements between the clay raw materials and the Neolithic ceramics of Piano dei Cardoni in Ustica and on what is known from the literature for the clays and the ceramics of Lipari.

deeper insight into the group of red-lustrous vessels conventionally classified as *Diana* ware.

Importantly, the red coloration of these ceramics is not solely attributable to firing conditions (oxidizing atmosphere) or post-firing mechanical polishing. Rather, it appears to have been intentionally achieved and enhanced through the application of specific preparatory coatings that intensify the red hue, as exemplified by specimens such as UCRD_25 (fig. 2.9).

Finally, the identification of two distinct ceramic fabric groups—both deriving from local clayey deposits differing in micrite content—suggests that these communities were mastering different raw materials and possessed a nuanced geological knowledge with implications perhaps for vessel functionality, but most likely for their appearance. Furthermore, the consistent use of particular clay-based coatings to produce contrasting surface finishes—micrite-rich for red-on-white painted ware versus iron-rich for lustrous red-burnished vessels—indicates deliberate technological choices embedded within broader esthetic and possibly cultural frameworks.

7 | Conclusions

The integrated approach combining traditional chronotypological and functional analyses with petro-chemical investigations of both ceramic vessels and local raw materials is applied here for the first time at a Neolithic site in Ustica. Ceramic production at Piano dei Cardoni emerges as a localized yet sophisticated craft system, shaped by environmental constraints, detailed material knowledge, and social practices embedded within a broader Neolithic network of interactions.

This study highlights the technological skills of the island's first pottery makers, who effectively exploited local resources and adapted their techniques to the volcanic soils of Ustica. The ceramic production was fully local, with no evidence of importation from Sicily or other nearby volcanic islands, while still reflecting integration within the wider Central Mediterranean cultural framework. Notable specificities arise from the exploitation of the island's unique clayey materials and the consistent use of relatively low firing temperatures.

Surface coating analyses reveal distinct treatments for burnished and painted wares, underscoring a deliberate esthetic focus on the vases dating to the mid-5th millennium BCE. This multidisciplinary approach, combining technological and decorative analyses, is essential to fully unlock the potential of ceramics as cultural indicators. The similarity between the red-on-light decoration at Piano dei Cardoni and those found in contemporary or earlier sites in Southern Italy further highlights the importance of expanded research into painted ceramics. Such a study could reveal underestimated or overlooked cultural networks until now.

Finally, future archaeometric analyses, especially of pottery from other chronological phases on Ustica, will be crucial for understanding local pottery-making traditions over time. These will enable assessment of technological continuities or shifts throughout the island's different periods of occupation.

Author Contributions

G. Montana: conceptualization, methodology, data curation, formal analysis, investigation, funding acquisition, writing – original draft, writing – review and editing, supervision. **C. Speciale:** conceptualization, investigation, funding acquisition, writing – original draft, writing – review and editing, project administration. **G. Battaglia:** Investigation, writing – review and editing. **L. Randazzo:** methodology, data curation, writing – original draft; writing – review and editing. **G. Carnevale**, **M. V. Antonopoulou:** formal analysis. **A. Magrì:** methodology, data curation, formal analysis, writing – original draft, writing – review and editing, supervision.

Acknowledgments

We thank the three anonymous reviewers for their careful reading of our manuscript and their insightful comments and suggestions. Postdoctoral contract to CS for the project "SILVA—Sicilian small IsLands Vegetation under the effect of the human Arrival" is part of the European Union's Horizon 2020 research and innovation program MSCA-COFUND R2STAIR (GA 101034349). Her research is also supported by the Spanish Ministry of Science and Innovation through the "Maria de Maeztu" excellence accreditation (CEX2019-000945-M) and CERCA, Centres de Recerca de Catalunya. Open access publishing facilitated by Universita degli Studi di Palermo, as part of the Wiley - CRUI-CARE agreement.

Conflicts of Interest

The authors declare no conflicts of interest.

References

Albero Santacreu, D. 2014. *Materiality, Techniques and Society in Pottery Production. The Technological Study of Archaeological Ceramics through Paste Analysis*. De Gruyter Open.

Amicone, S., P. S. Quinn, M. Marić, N. Mirković-Marić, and M. Radivojević. 2019. *Tracing Pottery-Making Recipes in the Prehistoric Balkans, 6th-4th Millennia BC*. Archaeopress Publishing.

Angeli, L., S. Legnaioli, C. Fabbri, et al. 2018. "Analysis of Serra d'Alto Figuline Pottery (Matera, Italy): Characterization of the Dark Decorations Using XRF." *Microchemical Journal* 137: 174–180. https://doi.org/10.1016/j.microc.2017.10.014.

Armetta, F., D. Giuffrida, M. C. Martinelli, V. Mollica Nardo, M. L. Saladino, and R. C. Ponterio. 2023. "Non-Invasive Investigation on Pigments of the Aeolian Islands Neolithic Pottery." *Materials Letters* 336: 133854. https://doi.org/10.1016/j.matlet.2023.133854.

Belfiore, C. M., M. A. Mastelloni, G. Barone, and P. Mazzoleni. 2022. "In Situ XRF Investigations to Unravel the Provenance Area of Corinthian Ware From Excavations in Milazzo (Mylai) and Lipari (Lipára)." *Heritage Science* 10: 32. https://doi.org/10.1186/s40494-022-00667-9.

Di Bella, M., M. A. Mastelloni, A. Baldanza, et al. 2019. "Archaeometric Constraints by Multidisciplinary Study of Richborough 527 Amphorae and Yellow Clays From the C.da Portinenti Pottery Workshop (Lipari Island, Italy)." *Archaeological and Anthropological Sciences* 11: 2957–2970. https://doi.org/10.1007/s12520-018-0727-2.

Bonomo, R., and V. Ricci. 2010. *Application of Unconformity-Bounded Stratigraphic (UBS) Units to the Geological Survey of the Volcanic Island Ustica (Italy)*. Geological Society of America.

Brunelli, D., S. T. Levi, P. Fragnoli, et al. 2013. "Bronze Age Pottery From the Aeolian Islands: Definition of Temper Compositional Reference Units by an Integrated Mineralogical and Microchemical Approach." *Applied Physics A* 113: 855–863. https://doi.org/10.1007/s00339-013-7775-3.

Capel, J., F. Huertas, A. Pozzuoli, and J. Linares. 2006. "Red Ochre Decorations in Spanish Neolithic Ceramics: A Mineralogical and Technological Study." *Journal of Archaeological Science* 33: 1157–1166. https://doi.org/10.1016/j.jas.2005.12.004.

Cinque, A., L. Civetta, G. Orsi, and A. Peccerillo. 1988. "Geology and Geochemistry of the Island of Ustica (Southern Tyrrhenian Sea)." *Rendiconti della società italiana di mineralogia e petrologia* 43: 987–1002.

Cultrone, G., C. Rodriguez-Navarro, E. Sebastian, O. Cazalla, and M. J. De la Torre. 2001. "Carbonate and Silicate Phase Reactions During Ceramic Firing." *European Journal of Mineralogy* 13: 621–634. https://doi.org/10.1127/0935-1221/2001/0013-0621.

Dawson, H. 2016. *Mediterranean Voyages: The Archaeology of Island Colonisation and Abandonment*. Routledge.

DiNapoli, R. J., and T. P. Leppard. 2018. "Islands as Model Environments." *Journal of Island and Coastal Archaeology* 13, no. 2: 157–160. https://doi.org/10.1080/15564894.2017.1311285.

Foresta Martin, F., and S. Furlani. 2021. "Geomorphology and Prehistoric Settlements on a Volcanic Island: The Case of Ustica (Palermo, Italy)." *Annals of Geophysics* 64, no. 5: VO550. https://doi.org/10.4401/ag-8703.

Furlani, S., F. Antonioli, D. Cavallaro, et al. 2017. "Tidal Notches, Coastal Landforms and Relative Sea-Level Changes During the Late Quaternary at Ustica Island (Tyrrhenian Sea, Italy)." *Geomorphology* 299: 94–106. https://doi.org/10.1016/j.geomorph.2017.10.004.

Giligny, F., E. Dolbunova, L. Gomart, A. Livingstone Smith, and S. Méry. 2021. "Contribution of the Ceramic Technological Approaches to the Anthropology and Archaeology of Pre- and Protohistoric Societies." In *Proceedings of the XVIII Union Internationale des Sciences Préhistoriques et Protohistoriques (UISPP) World Congress*, 1–3. Archaeopress Publishing.

Gliozzo, E. 2020. "Ceramic Technology. How to Reconstruct the Firing Process." *Archaeological and Anthropological Sciences* 12: 260. https://doi.org/10.1007/s12520-020-01133-y.

Karunadasa, K. S. P., C. H. Manoratne, H. M. T. G. A. Pitawala, and R. M. G. Rajapakse. 2019. "Thermal Decomposition of Calcium Carbonate (Calcite Polymorph) as Examined by In-Situ High-Temperature X-Ray Powder Diffraction." *Journal of Physics and Chemistry of Solids* 134: 21–28. https://doi.org/10.1016/j.jpcs.2019.05.023.

Laviano, R., and I. Muntoni. 2009. "Produzione e circolazione della ceramica 'Serra d'Alto' nel V millennio a.C. in Italia sud-orientale." In *Le classi ceramiche. Situazione degli studi., Atti della 10^ Giornata di Archeometria della Ceramica*, edited by S. Gualtieri, B. Fabbri and G. Bandini, 57–72. Edipuglia.

Laviano, R., and I. M. Muntoni. 2011. "La ceramica neolitica in Puglia (Italia): stato dell'arte e prospettive della ricerca archeometrica." In *Itinerari di ricerca dall'antichità all'epoca della globalizzazione*, edited by A. Alvarez-Hernandez, A. Campione and G. Otranto, 49–67. Sodalitas.

Levi, S. T., V. Cannavò, and M. C. Martinelli, et al. 2020. "Tradition and Innovation: Pre and Protohistoric Pottery at Lipari in a Wider Environmental and Cultural Perspective." *Rivista di Scienze Preistoriche* 70: 5–28.

Levi, S. T., and I. M. Muntoni. 2014. *L'archeometria della ceramica in Italia: storia degli studi e prospettive della ricerca*, 535–542. Studi di Preistoria e Protostoria, 1. Casalini.

MacArthur, R. H., and E. O. Wilson. 2016. *The Theory of Island Biogeography*. Princeton University Press.

Maggetti, M., C. Neururer, and D. Ramseyer. 2011. "Temperature Evolution Inside a Pot During Experimental Surface (Bonfire) Firing." *Applied Clay Science* 53, no. 3: 500–508. https://doi.org/10.1016/j.clay.2010.09.013.

Magrì, A., C. Speciale, G. Montana, R. Mentesana, and G. Battaglia. 2023. "Piano dei Cardoni (Ustica, Palermo): primi risultati dell'analisi sulle ceramiche del Neolitico Medio-Recente", in La ceramica in Sicilia dalla Preistoria all'Età Contemporanea. Atti del II Convegno Internazionale. 33–41. Edizioni Quasar.

Maniatis, Y., and M. S. Tite. 1981. "Technological Examination of Neolithic-Bronze Age Pottery From Central and Southeast Europe and From the Near East." *Journal of Archaeological Science* 8: 59–76.

Mannoni, T. 1980. "Analisi delle ceramiche dipinte neolitiche di Lipari." *Meligunıs Lipara* 4: 870–875.

Martin, F., and S. Furlani. 2021. "Geomorphology and Prehistoric Settlements on a Volcanic Island: The Case of Ustica (Palermo, Italy)." *Annals of Geophysics* 64, no. 5: VO550. https://doi.org/10.4401/ag-8703.

Martinelli, M. C. 2020. *Isole vicine. L'arcipelago delle isole Eolie e le comunità umane nella preistoria mediterranea*. Edizioni di Storia e Studi sociali.

Matthew, A. J. 1991. "Spots Before the Eyes: New Comparison Charts for Visual Percentage Estimation in Archaeological Material." In *Recent Developments in Ceramic Petrology*, edited by A. Middleton and I. Freestone, 399–409. British Museum Occasional Paper.

Mirabella, A., M. Egli, S. Raimondi, and D. Giaccai. 2005. "Origin of Clay Minerals in Soils on Pyroclastic Deposits in the Island of Lipari (Italy)." *Clays and Clay Minerals* 53, no. 4: 409–421. https://doi.org/10.1346/CCMN.2005.0530409.

Montana, G. 2020. "Ceramic Raw Materials: How to Recognize Them and Locate the Supply Basins—Mineralogy, Petrography." *Archaeological and Anthropological Sciences* 12: 175. https://doi.org/10.1007/s12520-020-01130-1.

Montana, G., B. Fabbri, S. Santoro, et al. 2007. "Pantellerian Ware: A Comprehensive Archaeometric Review." *Archaeometry* 49, no. 3: 455–481. https://doi.org/10.1111/j.1475-4754.2007.00314.x.

Montana, G., L. Randazzo, M. G. Morticelli, V. Baldoni, and B. Bechtold. 2022. "The Production of Western Greek Amphorae in Agrigento (Southern Sicily): An Archaeometric and Archaeological Characterisation of the Late 6th-4th Centuries BCE Series." *Journal of Archaeological Science: Reports* 45: 103627. https://doi.org/10.1016/j.jasrep.2022.103627.

Muntoni, I., and R. Laviano. 2008. "Archaeometric Data on Production and Circulation of Neolithic Serra d'Alto Ware in Southern Italy During the Fifth Millennium BC." *ArcheoSciences* 32: 125–135. https://doi.org/10.4000/archeosciences.1032.

El Ouahabi, M., L. Daoudi, F. Hatert, and N. Fagel. 2015. "Modified Mineral Phases During Clay Ceramic Firing." *Clays and Clay Minerals* 63: 404–413. https://doi.org/10.1346/CCMN.2015.0630506.

Peccerillo, A. 2005. "Plio-Quaternary." In *Volcanism in Italy*, 365. Springer-Verlag.

Peters, T., and R. Iberg. 1978. "Mineralogical Study of the Firing Characteristics of Brick Clays." *American Ceramic Society Bulletin* 57, no. 503–505: 509.

Prillo, V. G., C. Speciale, and R. Miccichè. 2021. "Insularity and Singularity: Exploitation of Animal Resources in Sicilian Insular and Inland Territories During Prehistoric Times." In *Proceedings of the 9th Postgraduate ZooArchaeology Forum (PZAF)*, 27–29. BAR Publishing Series.

Quinn, P. S. 2013. *Ceramic Petrography: The Interpretation of Archaeological Pottery & Related Artefacts in Thin Section*. Archaeopress.

Roux, V. 2019. *Ceramics and Society. A Technological Approach to Archaeological Assemblages*. Springer.

Shepard, F. P. 1954. "Nomenclature Based on Sand-Silt-Clay Ratios." *Journal of Sedimentary Research* 24, no. 3: 151–158.

Speciale, C., V. G. Prillo, I. Arienzo, and R.Micciché (in press). "The Domestication of a Small Island: Animals and Plants During the First Human Colonization of Ustica (Sicily, Italy)." Rivista di Scienze Preistoriche.

Speciale, C., F. de Angelis, A. Magrì, et al. 2024. "The Neolithic Site of Piano dei Cardoni (Ustica, Palermo) and the Chronology of Sicily Between the Mid-6th and the End of the 5th Millennium BCE." *Rivista di Scienze Preistoriche* 74, no. S4: 141–155.

Speciale, C., G. Battaglia, N. Larosa, and A. Magrì. 2022. "Piano dei Cardoni (Ustica, Palermo)." *Notiziario di Preistoria e Protostoria* 8, no. 2: 79–81.

Speciale, C., K. P. Freund, S. de Vita, et al. 2021. "Obsidian From the Site of Piano dei Cardoni, Ustica (Palermo, Italy): Preliminary Results on the First Occupation of the Island." *Open Archaeology* 7, no. 1: 273–290. https://doi.org/10.1515/opar-2020-0140.

Speciale, C., N. Larosa, G. Battaglia, and S. Vassallo. 2019. "Piano dei Cardoni, Ustica (Palermo)." *Notiziario di Preistoria e Protostoria* 6, no. 2: 62–64.

Speciale, C., N. Larosa, F. Spatafora, et al. 2023. "Archaeobotanical and Historical Insights on Some Steps of Forest Cover Disruption at Ustica Island (Sicily, Italy) From Prehistory Until Present Day." *Environmental Archaeology* 28, no. 4: 312–327. https://doi.org/10.1080/14614103.2021.1962578.

Speciale, C., G. Montana, R. Mentesana, et al. 2021. "Materials and Tools Across Volcanoes: Exploitation of Georesources in Piano dei Cardoni (Ustica, Italy) During Prehistory." *Annals of Geophysics* 64: VO552. https://doi.org/10.4401/ag-8684.

Tite, M. S., and Y. Maniatis. 1975. "Scanning Electron Microscopy of Fired Calcareous Clays." *Transactions and Journal of the British Ceramic Society* 74: 19–22.

de Vita, S. 1993. "Assetto geologico-strutturale ed evoluzione vulcanologica dell'isola di Ustica (stratigrafia, tettonica e meccanismi eruttivi)." PhD thesis, Napoli.

de Vita, S., and F. Foresta Martin. 2017. "The Palaeogeographic Setting and the Local Environmental Impact of the 130 ka Falconiera Tuff-Cone Eruption (Ustica Island, Italy)." *Annals of Geophysics*60, no. 2: S0224. https://doi.org/10.4401/ag-7113.

de Vita, S., G. Guzzetta, and G. Orsi. 1995. "Deformational Features of the Ustica Volcanic Island in the Southern Tyrrhenian Sea (Italy)." *Terra Nova* 7: 623–629.

de Vita, S., M. A. Laurenzi, G. Orsi, and M. Voltaggio. 1998. "Application of 40Ar/39Ar and 230Th Dating Methods to the Chronostratigraphy of Quaternary Basaltic Volcanic Areas: The Ustica Island Case History." *Quaternary International* 47/48: 117–127.

Williams, J. L. 1980. "A Petrological Examination of The Prehistoric Pottery from the Excavations in the Castello and Diana Plain of Lipari." In *Meligunìs Lipára, IV. L'acropoli di Lipari :nella preistoria*, edited by L. Bernabò Brea and M. Cavalier, 847–868. L'Erma di Bretschnider.

Williams, J. L., and S. T. Levi. 2008. "The Ausonian Pottery of Lipari (Aeolian Islands, Sicily)—A Typological and Petrological Assessment." *Proceedings of the Prehistoric Society* 74: 141–170. https://doi.org/10.1017/S0079497X00000177.

Supporting Information

Additional supporting information can be found online in the Supporting Information section.
Supplementary Table 1A: Piano dei Cardoni, Ustica: ceramic samples without micrite lumps (19 on 28 samples – 68%). **Supplementary Table 1B:** Piano dei Cardoni, Ustica: ceramic samples with micrite lumps (9 on 28 samples – 32%). **Supplementary Table 2:** Schematic description under the polarizing microscope of the compositional and textural characteristics of the studied samples (fired local clay raw materials and ceramics). **Supplementary Table 3:** Chemical composition of the studied samples (fired local clay raw materials and ceramics); PML = Pedogenic Micrite Lumps. RSD = Relative Standard Deviation. The concentrations of oxides of major elements are expressed in % weight (wt.%), whereas trace elements are expressed in ppms.